TU Delft

Delft University of Technology

Daily flow simulation in Thailand Part I

Testing a distributed hydrological model with seamless parameter maps based on global data

Wannasin, C.; Brauer, C.C.; Uijlenhoet, R.; van Verseveld, W.J.; Weerts, Albrecht H.

DOI
10.1016/j.ejrh.2021.100794

Publication date
2021

Document Version
Final published version

Published in
Journal of Hydrology: Regional Studies

Citation (APA)
Wannasin, C., Brauer, C. C., Uijlenhoet, R., van Verseveld, W. J., & Weerts, A. H. (2021). Daily flow simulation in Thailand Part I: Testing a distributed hydrological model with seamless parameter maps based on global data. *Journal of Hydrology: Regional Studies*, *34*, 1-19. Article 100794. https://doi.org/10.1016/j.ejrh.2021.100794

Important note
To cite this publication, please use the final published version (if applicable).
Please check the document version above.

Copyright
Other than for strictly personal use, it is not permitted to download, forward or distribute the text or part of it, without the consent of the author(s) and/or copyright holder(s), unless the work is under an open content license such as Creative Commons.

Takedown policy
Please contact us and provide details if you believe this document breaches copyrights.
We will remove access to the work immediately and investigate your claim.

This work is downloaded from Delft University of Technology.
For technical reasons the number of authors shown on this cover page is limited to a maximum of 10.

Journal of Hydrology: Regional Studies 34 (2021) 100794

Contents lists available at ScienceDirect

Journal of Hydrology: Regional Studies

journal homepage: www.elsevier.com/locate/ejrh

Daily flow simulation in Thailand Part I: Testing a distributed hydrological model with seamless parameter maps based on global data

C. Wannasin [a,*], C.C. Brauer [a], R. Uijlenhoet [a,b], W.J. van Verseveld [c], A.H. Weerts [a,d]

[a] Hydrology and Quantitative Water Management Group, Wageningen University and Research, P.O. Box 47, 6700AA Wageningen, The Netherlands
[b] Department of Water Management, Faculty of Civil Engineering and Geosciences, Delft University of Technology, P.O. Box 5048, 2600GA Delft, The Netherlands
[c] Catchment and Urban Hydrology, Department of Inland Water Systems, Deltares, P.O. Box 177, 2600MH Delft, The Netherlands
[d] Operational Water Management, Department of Inland Water Systems, Deltares, P.O. Box 177, 2600MH Delft, The Netherlands

ARTICLE INFO

Keywords:
Wflow_sbm
Reservoir modeling
Data scarcity
Global forcing data
Pedotransfer function
Chao Phraya basin

ABSTRACT

Study region: Upper region of the Greater Chao Phraya River (GCPR) basin in Thailand.
Study focus: This study presents a (~1 km resolution) distributed hydrological model, wflow_sbm, with global spatial data and parameterization for estimating daily streamflow in the upper GCPR basin, with the aim to overcome in situ data scarcity often occurring in Southeast Asia. We forced the model with the MSWEP V2 precipitation and eartH2Observe potential evapotranspiration datasets. Seamless distributed parameter maps based on pedotransfer functions (PTFs) and literature review were applied to bypass calibration. Only the *KsatHorFrac* parameter determining the lateral subsurface flow was calibrated. A target storage-and-release-based reservoir operation module (ROM) was implemented to simulate reservoir releases. We compared the simulated daily streamflows obtained from different PTFs and evaluated the model performance in the period 1989–2014.
New hydrological insights for the region: The global-data-driven wflow_sbm model can reconstruct daily streamflow in the upper GCPR basin, especially for natural catchments (KGE = 0.78). The ROM can capture the seasonal variability of reservoir releases, but not very accurately at the daily timescale (KGE = 0.43) since the actual reservoir operations are too complex. Different PTFs and *KsatHorFrac* values only introduce little uncertainty in the streamflow results. Therefore, the proposed model provides an opportunity for streamflow estimation in other ungauged or data-scarce basins in Southeast Asia. Nonetheless, the difficulty in the reservoir system modeling reflects the necessity of better understanding of human intervention on daily streamflow.

1. Introduction

Floods and droughts have caused profound damage at the global scale, amplified by climate change and land use change (Chang and Franczyk, 2008; Dai, 2011; Ward et al., 2013; Bagley et al., 2014). These hydrological hazards have dramatically increased in many regions and are expected to become more frequent and severe in the future (Trenberth et al., 2014; Winsemius et al., 2016).

* Corresponding author.
E-mail address: chanoknun.wannasin@wur.nl (C. Wannasin).

https://doi.org/10.1016/j.ejrh.2021.100794
Received 3 August 2020; Received in revised form 21 January 2021; Accepted 13 February 2021
Available online 9 March 2021
2214-5818/© 2021 The Authors. Published by Elsevier B.V. This is an open access article under the CC BY-NC-ND license (http://creativecommons.org/licenses/by-nc-nd/4.0/).

Southeast Asia (SEA) is a region that is exceptionally prone to both floods (Hirabayashi et al., 2013; Ceola et al., 2014; Arnell and Gosling, 2016) and droughts (Cook et al., 2010; Dai, 2013; Trenberth et al., 2014). The vulnerability of SEA is partially due to the changes in monsoon dynamics and partially due to socio-economic development, such as urbanization, deforestation and cultivation, in the developing countries. Mitigating these hydrological hazards in SEA requires rational water resource planning and management at the basin scale.

The Greater Chao Phraya River (GCPR) basin in Thailand is representative of the vulnerable and highly regulated river basins in SEA, considering its agriculture and water resource managements. Despite the water regulation by several multipurpose reservoirs, the basin has still experienced hydrological hazards almost annually. The most catastrophic floods occurred in 1995, 2006 and 2011, followed by serious droughts in 2013–2016 (Takeda et al., 2016; Kinouchi et al., 2018). The 2011 GCPR flood was one of the most devastating hazards recorded in SEA, with an inundated area of over 30,000 km^2, 13 million people affected and more than 800 fatalities (Komori et al., 2012). This calls for the development of comprehensive hydrological models for the basin, particularly at the (sub)daily timescale, to assist early warning and mitigation of floods and droughts. Similar extreme events have occurred in neighboring countries, such as Vietnam and Myanmar (Luu et al., 2018; Myo Lin et al., 2018). Thereupon, knowledge obtained from hydrological modeling in the GCPR basin can also contribute to water resource management in other SEA basins.

Several hydrological models have been developed over the past decades for better understanding of rainfall-runoff processes and have become important tools for scenario simulations, predictions and decision making for river basin management (e.g., Mysiak et al., 2005; Ajami et al., 2008; Cloke and Pappenberger, 2009). Hydrological models can be classified as lumped or distributed according to the spatial representation (Singh and Woolhiser, 2002). Lumped models mathematically simplify the rainfall-runoff processes in a basin with spatially averaged parameters. Lumped model parameters have to be calibrated as they cannot be obtained from direct measurements, thus limiting model applications to gauged basins (Crawford, 1966). With improvements in computer technologies, distributed models have been developed (Singh and Woolhiser, 2002), which allow mathematically describing the rainfall-runoff processes in a spatially distributed way. This model type uses parameters directly related to physical characteristics of the basin (e.g., topography, soil, land cover and river network) and takes into account spatial heterogeneity in both physical characteristics and meteorological inputs. Therefore, distributed models potentially provide additional and more correct description of hydrological processes in the basin compared to lumped models (Refsgaard and Knudsen, 1996; Wicks and Bathurst, 1996). Since distributed models can fulfill various needs in spatial modeling, such as flood and drought extents, they have been widely used in water resource planning and management.

Despite their benefits, distributed models are much more complex and difficult to apply than lumped models. Firstly introduced in the 1970s, the distributed models were expected to be used without prior calibration by directly determining model parameters from field data (Abbott et al., 1986). This means the model results significantly depend on the accuracy of geospatial and spatial meteorological input data (Gourley and Vieux, 2006). In practice, however, these in situ data are not always available, especially for ungauged or sparsely gauged basins in developing countries, including in SEA (Grayson and Blöschl, 2001). Therefore, like lumped models, some distributed parameters are still subject to calibration (Refsgaard, 1997). Calibrating a distributed model generally sets different parameter values to different grid cells, which poses a high risk of overparameterization, requires enormous computational demands at fine resolutions and obstructs model applications in large basins (Beven, 2006).

Fortunately, the advancement in remote sensing and geographic information system (GIS) data, including soils, land cover and climate, in recent decades can potentially complement some absences of field data and provide new means of spatial calibration and validation. Many remote sensing and GIS data are available in global public domains, with relatively high spatial and temporal resolutions (Fortin et al., 2001; Skidmore, 2017). With the availability of global high-resolution soil data (e.g., Hengl et al., 2017), the recent attention has also been focused on pedotransfer functions (PTFs) for soil-related parameterization. Traditionally used in soil science, PTFs characterize soil hydraulic properties using predictive functions and structural soil data (Van Looy et al., 2017). Therefore, they have great potential to facilitate soil-related parameters, such as the water retention characteristic and hydraulic conductivity, in distributed models (Zhao et al., 2016a; Imhoff et al., 2020). Together with powerful computer resources, we can attempt to maximize the use of remote sensing, GIS and PTFs data in order to minimize the number of calibrated parameters in distributed models. This offers an opportunity to develop more feasible and reliable distributed models for basins with data scarcity like in SEA.

In basins that are highly regulated by dammed reservoirs, hydrological models also need explicit reservoir operation components. This is yet another motivation to use distributed hydrological models in this context. Failure to represent reservoir operations limits the model performances and their applicability in scenario analyses, with climate, land use and operation changes (Yassin et al., 2019). The existing reservoir operation schemes in hydrological models are categorized into four types: natural lake, inflow- and demand-based, data-driven and target storage-and-release-based (Yassin et al., 2019). The natural lake method is limited to uncontrolled reservoirs (without dams). The inflow- and demand-based methods determine reservoir releases as a function of inflows and downstream water demands, but cannot account for reservoir operations in detail. The data-driven methods can simulate reservoir releases more accurately, but cannot provide insight into the reservoir operation mechanisms due to their black box characteristics. The target storage-and-release-based methods consider reservoir storage zoning and adjust reservoir releases as a function of dynamic target storage, so-called operating rule curves. The main challenge for this type of methods is the large amount of required data, such as the storage zone setting and actual rule curves of each reservoir, that are not always documented or easy to obtain. However, considering the growing availability of global data, the target storage-and-release-based methods seems to be the most promising for the simulation of multipurpose reservoirs at the daily timescale (e.g., Zhao et al., 2016b; Zajac et al., 2017; Yassin et al., 2019).

Previous studies have investigated the performance of various distributed models on the monthly and daily streamflow simulations in the GCPR basin and other highly regulated basins in SEA (e.g., Kite, 2000; Kure and Tebakari, 2012; Sayama et al., 2015). Many of

them have utilized global geospatial data (e.g., Thanapakpawin et al., 2007; Vo and Gourbesville, 2016; Bhagabati and Kawasaki, 2017; Livneh et al., 2017). Some studies have further implemented daily meteorological data from global databases to force the models instead of using gauged data, and they have shown promising performances. (e.g., Wang et al., 2016; Liu et al., 2017; Li et al., 2019; Yuan et al., 2019). Few studies have implemented the target storage-and-release-based methods (e.g., Kite, 2001; Mateo et al., 2014). However, all mentioned studies still needed to calibrate a few to several distributed parameters that are related to soil, land cover or reservoir operation. To date, no study has applied distributed models with global parameterization to simulate daily streamflow in the GCPR and other SEA basins.

This study aims to develop a (~1 km resolution) distributed hydrological model with global spatial data and parameterization for estimating daily streamflow in the upper region of the GCPR basin, to overcome in situ data scarcity often occurring in SEA and to minimize the model calibration. We used the wflow_sbm model (Schellekens et al., 2019), which has shown good performance in basins across a large range of elevations and drainage areas (e.g., López López et al., 2016; Hassaballah et al., 2017; Giardino et al., 2018; López López, 2018; Gebremicael et al., 2019; Imhoff et al., 2020). The utilized global remote sensing and GIS data included (i) static geospatial data from global databases; (ii) meteorological forcing data from the global reanalysis; (iii) seamless distributed maps for soil-related parameters obtained with PTFs and (iv) seamless distributed maps for land cover-related parameters obtained from literature review and global databases. Model results from different PTFs were investigated. A reservoir operation module (ROM) with a target storage-and-release-based method was implemented with a minimum number of parameters and accessible operating rule curve data without calibration. The performance of the global-data-driven wflow_sbm model with the ROM were evaluated in both natural and regulated catchments.

The paper is organized as follows. In Section 2, we introduce the study area. In Section 3, we summarize the selected global datasets. The methodology, including the wflow_sbm model, parameterization, reservoir operation module and model evaluation, are presented in Section 4. Next, the results on model performance are shown in Section 5. The results are then discussed in Section 6, followed by the conclusion and outlook in Section 7.

2. Study area

The Greater Chao Phraya River basin (GCPR) is Thailand's largest and most important basin with respect to land and water resource development. The entire basin covers an area of approximately 158,600 km^2, accounting for 30% of the country's surface area (Fig. 1).

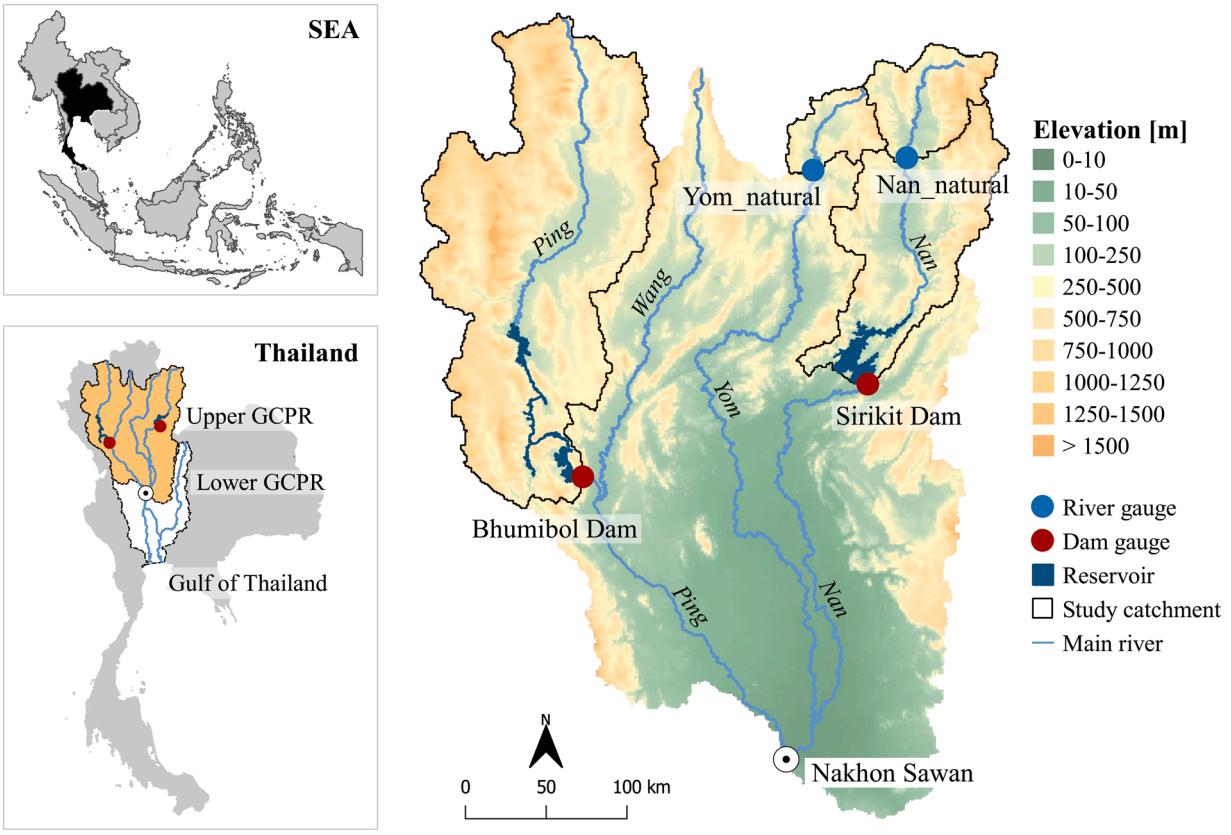

Fig. 1. Overview of the study area. The top left panel shows the location of Thailand in Southeast Asia, the bottom left panel shows the location of the GCPR basin in Thailand, and the right panel shows the upper GCPR basin with the spatial distribution of reservoirs and study catchments.

The basin can be divided geographically into the upper region (66%) and lower region (34%). This study focused on the upper region where the main reservoirs are located. This region consists of four sub-basins, namely the Ping River (34,500 km^2), Wang River (10,800 km^2), Yom River (24,000 km^2), and Nan River (34,700 km^2). The elevation of the upper region ranges from 22 to 2534 m above sea level. The four rivers merge at Nakhon Sawan and form the origin of the Chao Phraya River. The river then drains through the lower region, with intensive rice cultivation and densely populated areas, before emptying into the Gulf of Thailand.

The climate of the upper GCPR basin is characterized by tropical monsoons and cyclones, contributing to the high seasonal variability of precipitation. The wet (rainy) season is when the southwest monsoons from the Indian Ocean, together with tropical cyclones from the Pacific Ocean and South China Sea, bring very humid air towards the basin, causing heavy rainfall from May to October. Therefrom, the northeast monsoons bring cool and dry air from the Siberian anticyclone, causing the dry season from November to April (Bachelet et al., 1992; Kripalani et al., 1995). Considering the seasonality, the Thai water-year is set as a period from April 1st of any given year to March 31st of the following year. From this point onward, we refer to water-year and water-yearly as year and yearly/annual (i.e., the year 2011 is from April 1st, 2011 to March 31st, 2012). The long-term yearly average of precipitation from 1989 to 2013 is 1060 mm. The highest yearly precipitation was recorded in 2011 (1449 mm) and the lowest in 1993 (841 mm). Most precipitation (86%) occurs in the rainy season. Accordingly, annual maximum daily flows often occur in September and October, while annual minimum daily flows mostly occur in January. The highest daily streamflow ever recorded at Nakhon Sawan was 5450 $m^3 s^{-1}$ (October 2006) and the lowest was 52 $m^3 s^{-1}$ (April 1994).

For the purposes of irrigation, hydropower generation and flood control, seven large dammed reservoirs have been constructed and operated in the upper GCPR basin over the past 55 years. The Bhumibol and Sirikit reservoirs (locations shown in Fig. 1) are the two largest ones in terms of storage capacity. They are currently managed by the Royal Irrigation Department of Thailand (RID) and the Electricity Generating Authority of Thailand (EGAT). Principle characteristics of the two reservoirs obtained from RID are presented in Table 1. Together, they account for 93% of the total reservoir capacity (24.7 billion m^3) in the upper region. Therefore, we focus on modeling the Bhumibol and Sirikit reservoirs in this study, with the assumption that the influences of the other five reservoirs on streamflow are insignificant at the basin scale.

To investigate the model performance, we selected two natural and two regulated catchments in the upper GCPR basin (catchment locations shown in Fig. 1). The natural catchments from the Nan and Yom headwaters were selected based on available data and will be called the Nan_natural (3546 km^2) and Yom_natural (2018 km^2). The regulated catchments represent the drainage areas from the headwater until the dam location and will be called the Sirikit catchment (13,155 km^2) and Bhumibol catchment (25,988 km^2).

3. Data

This study required geospatial data, meteorological data and hydrological data for the model setup and validation. The geospatial data were used to represent the physical characteristics of the basin in the wflow_sbm model. The meteorological data were used as model driving forces. The hydrological data were used in the parameter optimization and result analyses. Most data were obtained from global databases as we attempted to overcome data scarcity in the study area, which is a common challenge in SEA.

The geospatial data comprised the Digital Elevation Model (DEM), land cover types, soil types and river network. The DEM was obtained from the Shuttle Radar Topography Mission (SRTM; Jarvis et al., 2008), the land cover from GLOBCOVER (Bontemps et al., 2011), the soil from SoilGrids (Hengl et al., 2017) and the river network from the Royal Irrigation Department (RID). The DEM and river network data were employed to create the distributed maps of basin boundary, local drainage direction, Strahler stream orders and river length per grid cell in the wflow_sbm model. These maps indicate the flow directions and control hydrological processes in a distributed way. In this study, the land cover and soil data were not directly used as model inputs, but were used in the estimation of global parameters (see Section 4.2).

The meteorological data for forcing the wflow_sbm model were precipitation (*P*) and potential evapotranspiration (*PET*). *P* data were obtained from the Multi-Source Weighted-Ensemble Precipitation Version 2 (MSWEP V2; Beck et al., 2019). The dataset was constructed using gauges, satellites and reanalyses, with corrections for distributional biases and systematic terrestrial *P* biases. It is available at high spatial (~10 km) and temporal (3-hourly) resolutions for the 1979–2017 period. *PET* data were obtained from the eartH2Observe database (Schellekens et al., 2017) as the successor of the WATCH-Forcing-Data-ERA-Interim (WFDEI) data (Weedon et al., 2014). They are offered with many calculation methods, of which we selected the FAO Penman-Monteith *PET* dataset (Allen

Table 1
Characteristics of the Bhumibol and Sirikit reservoirs.

Characteristic	Bhumibol	Sirikit
River	Ping	Nan
Dam type	Gravity arch	Earthfill
Operation since	1964	1977
Dam height (m)	154	134
Mean daily inflow ($m^3 s^{-1}$)	178	184
Mean daily outflow ($m^3 s^{-1}$)	170	179
Minimum daily outflow recorded ($m^3 s^{-1}$)	0	0
Maximum daily outflow recorded (*ResMaxQ*) ($m^3 s^{-1}$)	746	809
Reservoir capacity (*ResMaxVol*) (billion m^3)	13.46	9.51
Reservoir surface area (*ResArea*) (km^2)	297	315

et al., 1998). It is also available at the high spatial (~10 km) and temporal (daily) resolutions for the 1979–2014 period (Sperna Weiland et al., 2015). Both the MSWEP V2 *P* and the eartH2Observe *PET* datasets have shown to produce promising model results in many hydrological and meteorological studies (e.g., Tarnavsky et al., 2018; Liu et al., 2019; Xu et al., 2019; Beck et al., 2017; Beck et al., 2020) and therefore were chosen to force the wflow_sbm model for the upper GCPR basin. Since we did not have to compute the *PET* nor account for snow processes within the model, other forcing data, such as temperature and solar radiation, were unnecessary.

The required hydrological data included observed daily streamflow at the outlets of the study catchments and reservoirs of interest, observed daily storage of each reservoir and dynamic operating rule curves of each reservoir. The data were provided by the Royal Irrigation Department of Thailand (RID) and the Electricity Generating Authority of Thailand (EGAT). The observed daily streamflow is the average of the observed hourly streamflow from 6.00 p.m. of the previous day to 6.00 p.m. of the defined day. Their availability varies among gauges (see Table 2). The reservoir operating rule curves consist of the long-term monthly target storage of each reservoir derived from the RID report and the long-term monthly target water demand that we manually extracted from the observed daily streamflow data of each reservoir (more detail in Section 4.3). In reality, these reservoir operating rule curves serve as guidelines for dam-operators.

4. Methodology

4.1. Wflow_sbm model

The wflow simple bucket model, so-called wflow_sbm, is a conceptual rainfall-runoff model in the spatially distributed wflow modeling platform, which is PCRaster and python based (Schellekens et al., 2019). The soil water processes of wflow_sbm are based on the Topog_SBM model (Vertessy and Elsenbeer, 1999). The flow processes for subsurface, overland and river flows are based on the kinematic wave approach that are comparable to the TOPKAPI (Todini and Ciarapica, 2002) and G2G (Bell et al., 2007) models. While topog_sbm is suitable for small areas, wflow_sbm is more widely applicable (Vertessy and Elsenbeer, 1999; Schellekens et al., 2019). In contrast to many conceptual models, wflow_sbm calculates the lateral subsurface flow explicitly and uses parameters that represent simplified physical characteristics of a basin (Vertessy and Elsenbeer, 1999). It has shown good performance in a broad range of applications (e.g., López López et al., 2016; Hassaballah et al., 2017; Giardino et al., 2018; López López, 2018; Gebremicael et al., 2019; Imhoff et al., 2020).

The scheme of wflow_sbm is illustrated in Fig. 2. The one-dimensional model is constructed on a grid cell network of eight flow directions (D8) for surface and subsurface flow routing, with the presence of both vertical and lateral flows. It has four main routines: (i) a precipitation-snow routine based on the HBV model (Lindström et al., 1997), (ii) a rainfall interception routine based on the modified Rutter model (Rutter et al., 1971, 1975) or Gash model (Gash, 1979), (iii) a soil water routine based on topog_sbm, and (iv) a flow generation routine with the kinematic wave function. Water enters each grid cell through the precipitation-snow routine and is transferred to the rainfall interception routine. Throughfall and streamflow infiltrate into the soil and flows between the stacked unsaturated zone and saturated zone. The soil column can also be divided into different layers to allow for transfer of water within the unsaturated zone (Brooks and Corey, 1964). Part of the water evaporates depending on soil water content and vegetation cover. The soil water routine assumes an exponential decay of the saturated hydraulic conductivity with soil depth (Beven and Kirkby, 1979). In the flow generation routine, the subsurface, overland and river flows are then routed according to the D8 direction.

Table 2
Annual sums of water fluxes for catchments and years of interest. The fluxes comprise the MSWEP V2 Precipitation (*P*), eartH2Observe potential evapotranspiration (*PET*) and observed streamflow (*Q*). Nan_natural and Yom_natural are headwater catchments, whereas Sirikit and Bhumibol are midstream catchments. Therefore, the latter also receive inflows from upstream, which is not shown here. Note that the *P*, *PET*, and *Q* data were obtained from independent measurements or calculations.

Catchment	Component (mm year^{-1})	Wet (2006)	Dry (2013)	Long-term average (1989–2013)
Nan_natural	*P*	1225	1116	1230
	PET	1069	1079	1032
	Q	856	572	766 (1994–2013)
Yom_natural	*P*	1121	1048	1099
	PET	1123	1132	1086
	Q	513	261	386 (1996–2013)
Sirikit	*P*	1377	1030	1111
	PET	1223	1216	1181
	Q	3160	1905	2814 (1989–1997, 2003–2013)
Bhumibol	*P*	1179	858	942
	PET	1099	1107	1092
	Q	1075	569	780
Upper Chao Phraya (entire upstream area of Nakhon Sawan)	*P*	1248	1044	1060
	PET	1220	1221	1189
	Q	373	146	211

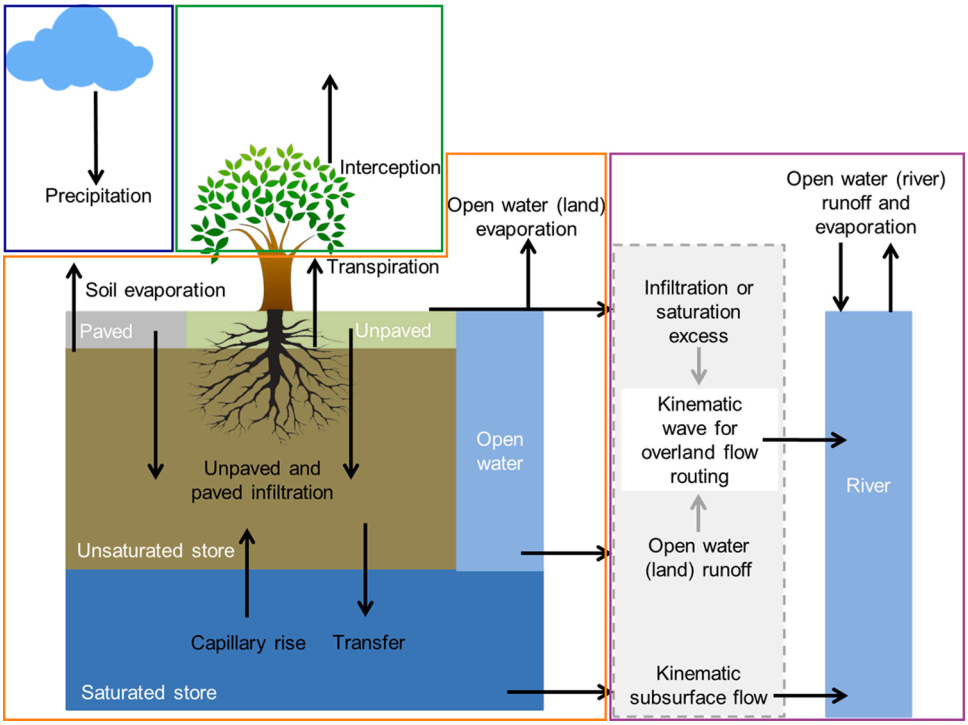

Fig. 2. Schematic structure of water processes and fluxes in the wflow_sbm model. The model includes four routines: precipitation-snow routine (blue), rainfall interception routine (green), soil water routine (orange) and runoff generation routine (purple) (adapted from Schellekens et al., 2019).

4.2. *Wflow_sbm parameterization*

Aiming to tackle the issues on data scarcity and overparameterization for the upper GCPR basin, we set up the wflow_sbm model with global parameterization. Recently, seamless distributed parameter maps at the global scale have been available for wflow_sbm (Schellekens et al., 2019; Imhoff et al., 2020). The main parameters and their sources for global parameterization used in this study are indicated in Table 3.

The seamless distributed maps of soil-related parameters for wflow_sbm were estimated with pedotransfer functions (PTFs) based on soil types from the SoilGrids database (Imhoff et al., 2020). They were initially applied to the Rhine basin and then regionalized to the global scale at the highest resolution of 250 m using the multi-parameter regionalization technique (MPR; Samaniego et al., 2010). Among five soil-related parameters (Table 3), users can choose different PTFs, such as Brakensiek (Brakensiek et al., 1984) and Cosby (Cosby et al., 1984) functions, to estimate two highly sensitive parameters, *KsatVer* (vertical saturated conductivity) and *M* (decay rate of *KsatVer*). We ran the wflow_sbm model simulations with the Brakensiek (PTF-B) and Cosby (PTF-C) parameter sets to investigate the effect of different PTFs on the model performance. The spatial comparison of both parameter sets for the upper GCPR basin is shown in Fig. 3.

The seamless distributed maps of land cover-related parameters for wflow_sbm were either estimated from literature review or taken directly from global databases, as indicated in Table 3. The parameter maps from literature review were collected as look-up tables and assigned to the land cover types of the GLOBCOVER database at its original resolution of 300 m. The parameter maps from global databases had different resolutions depending on their sources. This application assumed that the uncertainty in land cover changes over the study period is negligible at the basin scale. Examples of the spatial distribution of parameters associated with the land cover types for the upper GCPR basin are shown in Fig. 4.

Other insensitive parameters of wflow_sbm were set as default values (Schellekens et al., 2019), leaving only one soil-related parameter, *KsatHorFrac* [–], to be calibrated. *KsatHorFrac* is the multiplication factor applied to *KsatVer* (vertical saturated conductivity) to calculate horizontal saturated conductivity for computing the lateral subsurface flow. This parameter compensates for anisotropy, small-scale (soil core) saturated hydraulic conductivity measurements that do not represent larger-scale hydraulic conductivity and smaller flow length scales (hillslope) in reality, which cannot be represented with the model resolution. The ratio of horizontal saturated conductivity to vertical saturated conductivity has been reported for catchments in temperate climates with typical values of 20–100 (Calver and Cammeraat, 1993; Refsgaard, 1997; Brooks et al., 2004; Weiler and McDonnell, 2007; Gauthier et al., 2009).

Table 3
Main wflow_sbm parameters and their sources for global parameterization (Imhoff et al., 2020). The full list of wflow_sbm parameters can be found in Schellekens et al. (2019).

Model parameter	Parameter interpretation	Source of value determination
Soil-related parameters (pedotransfer functions; PTFs)		
c (at different depths)	Power coefficient based on the pore size distribution index used for computing vertical unsaturated flow (–)	Rawls and Brakensiek (1989)
KsatVer	Vertical saturated conductivity (mm day^{-1})	Brakensiek et al. (1984), Cosby et al. (1984)
M	Decay rate of KsatVer with depth (mm)	Fitting exponential function between KsatVer and depths of SoilGrids soil layers
thetaR	Residual water content (–)	Tóth et al. (2015)
thetaS	Saturated water content (–)	Tóth et al. (2015)
Land cover-related parameters (literature review)		
Kext	Extinction coefficient in the canopy gap fraction equation (–)	Assigned value per land cover type from Van Dijk and Bruijnzeel (2001)
LAI	Long-term monthly average leaf-area index (–)	Derived directly from Myneni et al. (2015), known as MOD15A2H MODIS data
N	Manning's roughness coefficient for the kinematic wave function for overland flow (m$^{-1/3}$ s)	Assigned value per land cover type from Engman (1986), Kilgore (1997)
N_river	Manning's roughness coefficient for the kinematic wave function for river flow (m$^{-1/3}$ s)	Assigned value per Strahler order from Liu et al. (2005)
RootingDepth	Maximum length of vegetation roots	Assigned value per land cover type from Zeng (2001)
Sl	Specific leaf storage for the interception module (mm)	Assigned value per land cover type from Pitman (1989), Liu (1998)
SoilThickness	Depth of the upper aquifer (mm)	Derived directly from Hengl et al. (2017)
Swood	Fraction of wood in the vegetation (–)	Assigned value per land cover type from Pitman (1989), Liu (1998)
WaterFrac	Fraction of surface water area per gridded cell (–)	Extracted from Bontemps et al. (2011)
Parameter subject to calibration		
KsatHorFrac	Multiplication factor applied to KsatVer for the horizontal saturated conductivity used for computing the lateral subsurface flow (–). This parameter compensates for anisotropy, small-scale KsatVer measurements (small soilcore) that do not represent larger-scale hydraulic conductivity, and model resolution (in reality smaller (hillslope) flow length scales).	Manual calibration

4.3. Reservoir operation module

We modeled the regulated outflows of the Sirikit and Bhumibol reservoirs by including a reservoir operation module (ROM) within the kinematic wave routing of wflow_sbm. To do so, grid cells of the dam locations and reservoir surface areas were indicated. The ROM is a reservoir water balance algorithm with a target storage-and-release-based operation method. The reservoir storage in the ROM is divided into four zones: inactive storage, conservation storage, flood control storage, and surcharge storage as illustrated in Fig. 5(A). The operating rule curve parameters include the target downstream water demand, target maximum storage and target minimum storage. As part of the distributed model, the ROM also requires parameters representing physical characteristics of each reservoir. As defined in Table 4, both operational and physical parameters are simplified and can be obtained directly from local data sources (RID and EGAT) or calculated from observed streamflow data without calibration. This allows for exploring the competence of available data. The values of the operating rule curve parameters for the Sirikit and Bhumibol reservoirs are shown in Fig. 5(B) and (C). The physical parameter values for each reservoir are indicated as the last three components in Table 1.

Although the ROM was developed as part of wflow_sbm (Schellekens et al., 2019), its complete description has not been published before. Therefore, we explain step-wise calculations of the ROM in brief here. Overall, at a given time step, the ROM updates the water storage state and computes a volume of water to be released with algorithms to meet a required demand, while also maintaining the storage at an optimal level, considering the target maximum and minimum storage. To calculate the change in the reservoir storage, the storage at the previous time step, upstream inflow, and precipitation and evaporation over the reservoir surface at the current time step are taken into account:

$$ResVol_t = ResVol_{t-1} + (ResInflow_t + ResP_t - ResET_t) \times \Delta t, \quad (1)$$

where *ResVol* is reservoir storage [m^3], *ResInflow* is upstream inflow [m^3 time step^{-1}], *ResP* is precipitation over the reservoir surface [m^3 time step^{-1}], *ResET* is evaporation over the reservoir surface [m^3 time step^{-1}], Δt is the computing time step (e.g., daily), t is the current time step and t-1 is the previous time step. Then, the current ResVol as a fraction of the reservoir maximum storage is computed:

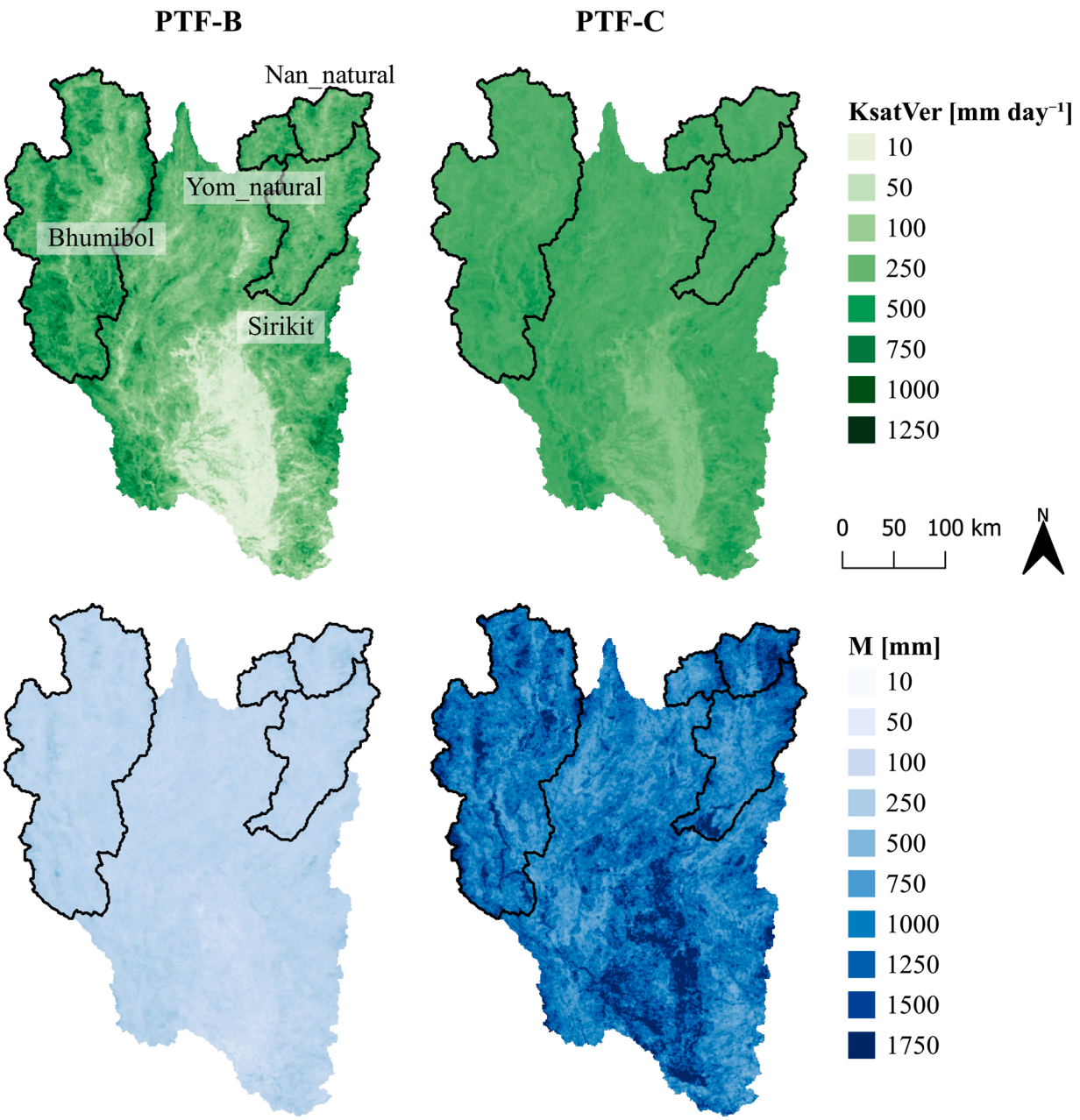

Fig. 3. Spatial distribution of soil-related parameters, *KsatVer* (upper panels) and *M* (lower panels), for the upper GCPR basin in comparison between the PTF-B (right) and PTF-C (left) methods at the ~1 km resolution. For parameter definitions, see Table 3. Boundaries of the four selected catchments are indicated in black color.

$$ResVolFrac_t = \frac{(ResVol_t + ResVol_{t-1})}{2 \times ResMaxVol}, \tag{2}$$

where *ResVolFrac* is the storage fraction [–], *ResMaxVol* is the reservoir maximum storage known as the flood control storage level [m^3]. The environmental outflow of a given reservoir, here called the demand release, is determined using a sigmoid curve to scale for the target storage and downstream water demand of the reservoir:

$$ResQdemand_t = \min(SF_t \times (DD_t \times \Delta t), ResVol_t), \tag{3}$$

where *ResQdemand* is the demand release [m^3], *SF* is the sigmoid curve factor [–] and *DD* is the downstream water demand [m^3 time step^{-1}], which is associated with the seasonality and often set on a long-term monthly basis (see Fig. 5(B)). *SF* influences the extent to

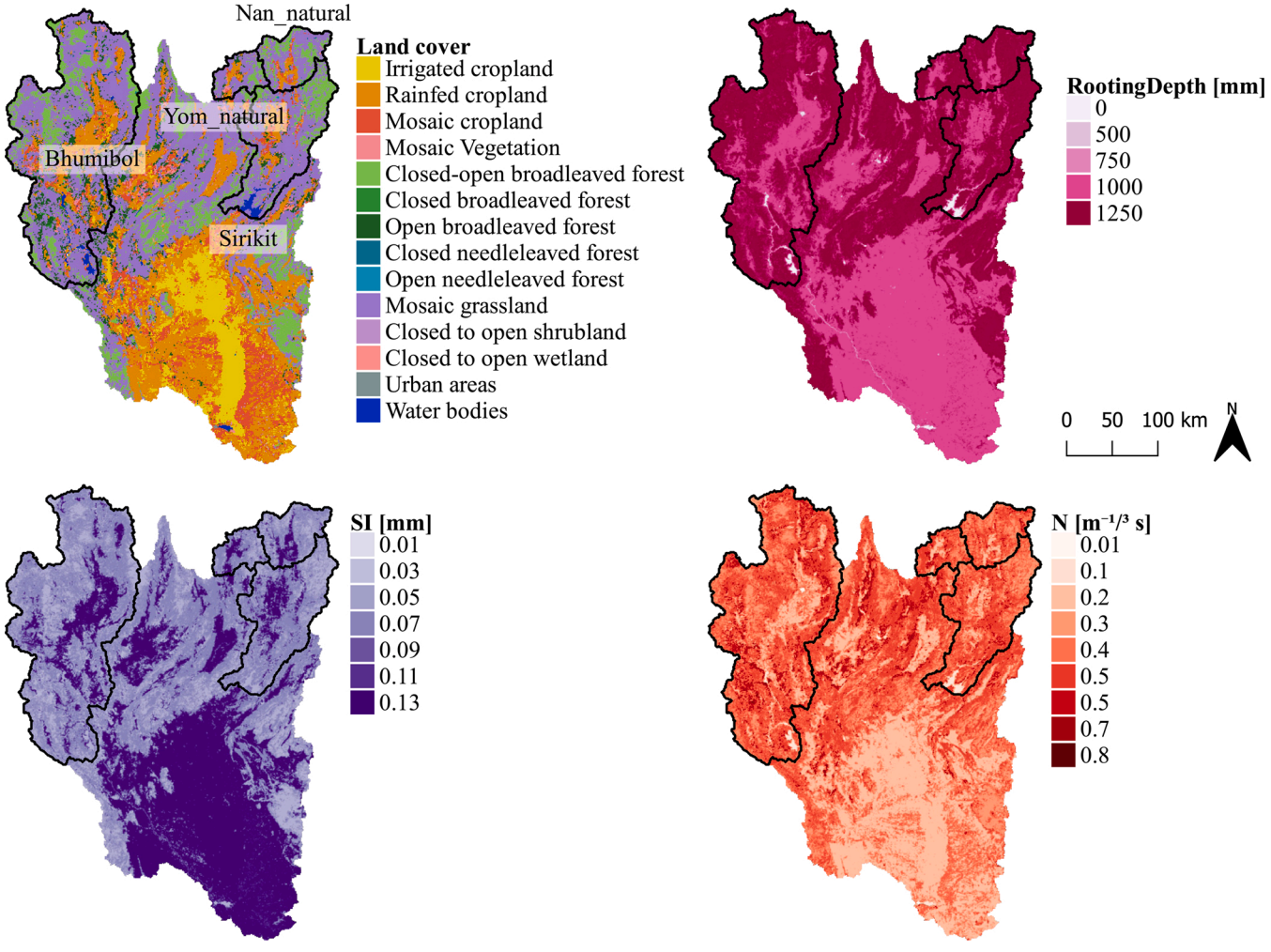

Fig. 4. Spatial distribution of land cover and its related parameters, *RootingDepth*, *SI* and *N*, for the upper GCPR basin at the ~1 km resolution. For parameter definitions, see Table 3. Boundaries of the four selected catchments are indicated in black color.

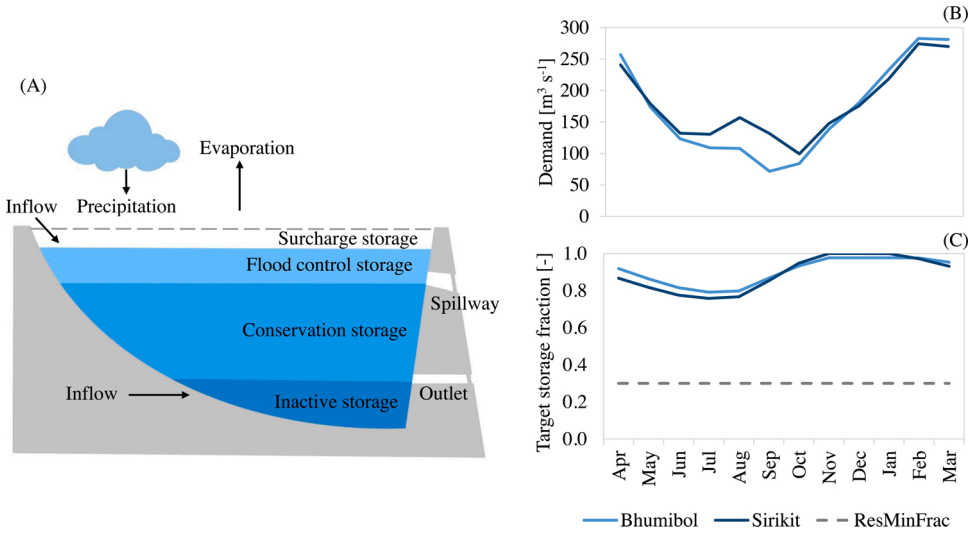

Fig. 5. Conceptual representation of the reservoir operation module (ROM), including reservoir storage zones (A) and operating rule curves for the Bhumibol and Sirikit reservoirs (B and C). Figure (B) represents the target downstream water demand of each reservoir, which is defined by the long-term monthly averages of reservoir outflow observations. Figure (C) represents the target storage as a fraction with respect to the maximum storage (flood control storage level). Colored lines indicate the fraction of long-term monthly target maximum storage (conservation storage level; *ResMaxFrac*) from the RID guideline. The dashed line indicates the fraction of target minimum storage (inactive storage level; *ResMinFrac*), which was set as 0.3 for both reservoirs.

Table 4
Reservoir parameters and their sources for parameterization (Schellekens et al., 2019). The values of the operating rule curve parameters for the Bhumilbol and Sirikit reservoirs are illustrated in Fig. 5. The values of the physical parameters are presented in Table 1.

Reservoir parameter	Parameter interpretation	Source of value determination
Operational (rule curve) parameters		
DD	Target of downstream water demand (m^3 time $step^{-1}$)	Long-term monthly average streamflow at a dam location (RID)
ResMaxFrac	Target of maximum storage (conservation storage level) as a fraction of *ResMaxVol*, ranging between 0 and 1 (–)	Long-term monthly target maximum storage (RID)
ResMinFrac	Target of minimum storage (inactive storage level) as a fraction of *ResMaxVol*, ranging between 0 and 1 (–)	Default setting
Physical parameters		
ResArea	Reservoir surface area used for estimating precipitation and evaporation (m^2)	RID
ResMaxQ	Maximum release capacity of a reservoir (m^3 time $step^{-1}$)	As the actual value is unknown, it was set as the maximum outflow in the historical record (RID)
ResMaxVol	Reservoir maximum storage (flood control storage level) (m^3)	RID

which *ResQdemand* increases or decreases, and is calculated by:

$$SF_t = \frac{1}{1 + \exp(-c \times (ResVolFrac_t - ResMinFrac))}, \quad (4)$$

where *c* is steepness of the sigmoid curve [–] and *ResMinFrac* is the target fraction of minimum storage, known as the inactive storage level [–] (see Fig. 5(C)). When the current *ResVolFrac* equals *ResMinFrac*, the argument of the exponential function is zero and the denominator becomes two. This implies that when the reservoir storage reaches the inactive storage level, which can occur in dry seasons, the reservoir only releases a *ResQdemand* equal to half of *DD*. *ResQdemand* decreases further as *ResVolFrac* drops below *ResMinFrac*. *ResVol* is updated after taking out *ResQdemand*. Subsequently, *ResVolFrac* is re-determined with Eq. (2).

The target fraction of maximum storage, known as the conservation storage level, is used as a guideline to not only maintain the active storage but also prevent the flood storage. It is conditional on water supply and demand throughout the year and often set on a long-term monthly basis (see Fig. 5(C)). The amount of water to be released from the reservoir to let *ResVol* continuously meet the conservation storage level is computed as:

$$ResQtarget_t = \max(0, ResVol_t - (ResMaxVol \times ResMaxFrac_t)), \quad (5)$$

where *ResMaxFrac* is the target fraction of maximum storage [–] and *ResQtarget* [m^3] is the target amount of water to be released to

meet *ResMaxFrac*. If *ResVol* is higher than *ResMaxVol*, the surcharge storage, *ResQspill* [m^3], is spilled to prevent dam failure:

$$ResQspill_t = \max(0, ResVol_t - ResMaxVol) \tag{6}$$

Eqs. (5) and (6) indicate that the reservoir release does not exceed *DD* unless *ResVol* is projected to surpass *ResMaxFrac* or *ResMaxVol*. In case of water excess, the amount of water to be released apart from the demand release is:

$$ResQextra_t = \min(ResQtarget_t, ResQspill_t, (ResMaxQ \times \Delta t) - ResQdemand_t), \tag{7}$$

where *ResQextra* [m^3] is the extra amount of water to be released and *ResMaxQ* [m^3 time $step^{-1}$] is the maximum release capacity of a reservoir (see Table 1). Since the environmental outflow (*ResQdemand*) is already calculated before updating *ResVol* (Eq. (3)), it is subtracted from the *ResMaxQ* amount in this step. Finally, the total release, *ResQtotal* [m^3 time $step^{-1}$], of the current time step is calculated according to:

$$ResQtotal_t = \frac{ResQdemand_t + ResQextra_t}{\Delta t} \tag{8}$$

4.4. Model application and evaluation

We applied the wflow_sbm model to the entire upper GCPR basin at a spatial resolution of approximately 1 km and temporal resolution of 3 h. The ~1 km grid cells could account for the areas of the two major reservoirs. The meteorological maps and seamless distributed parameter maps were upscaled or downscaled to the target resolution with parameter-specific upscaling procedures (Imhoff et al., 2020). Although our study focused on the daily timescale, we ran the model at the 3-hourly time step to be able to calculate the model results at the daily timescale using the same aggregation period as applied in the daily observations (6.00 p.m.–6.00 p.m.). The daily *PET* data were divided into 3-hourly data using hourly fractions.

We manually calibrated *KsatHorFrac* for the years 2010–2011, which contain extremely wet and dry periods. The parameter was calibrated separately for the PTF-B and PTF-C soil-related parameter sets, with the parameter values ranging from 100 to 800. We then validated the optimized *KsatHorFrac* values for the period of 1989–2013, excluding 2010–2011. We used 2006 and 2013 as the representative years for wet and dry conditions in the upper GCPR basin. The hydro-meteorological details of the extreme years and the entire study period for the selected four catchments in the upper GCPR basin are shown in Table 2.

The Kling Gupta efficiency (KGE; Gupta et al., 2009) was used as the objective function to optimize the *KsatHorFrac* parameter and to evaluate the accuracy of the wflow_sbm model and the ROM at the daily timescale. The KGE is the combination of three criteria that assess different hydrological dynamics (correlation, variability error and bias error), given by

$$\mathrm{KGE} = 1 - \sqrt{(r-1)^2 + (\alpha-1)^2 + (\beta-1)^2}, \tag{9}$$

where r is the Pearson correlation coefficient between simulated streamflow and observed streamflow (giving the error in the dynamics), α is the ratio of the standard deviation of simulated streamflow over the standard deviation of observed streamflow (giving the error in the variability), and β is the ratio between the mean simulated streamflow and the mean observed streamflow (giving the bias). The KGE ranges from $-\infty$ to 1, with an ideal value at unity when all three components are equal to 1 (Gupta, 2009).

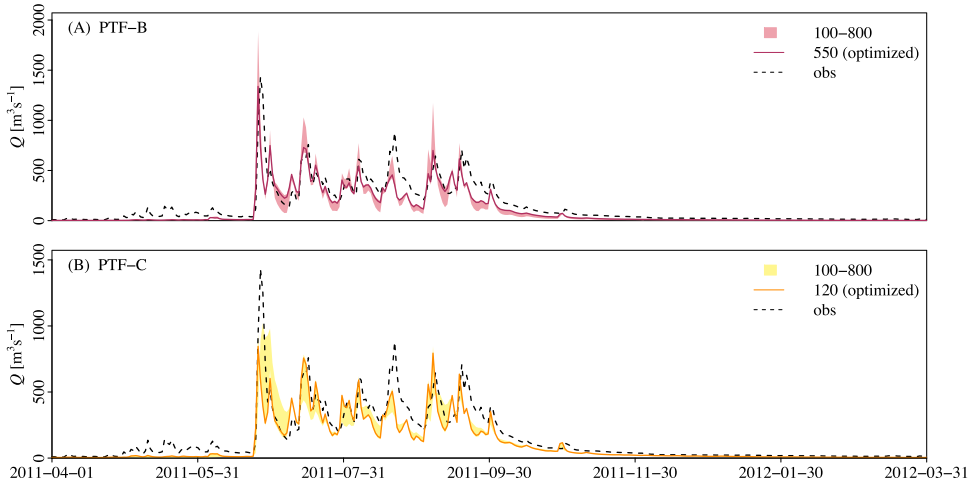

Fig. 6. Simulated and observed daily streamflows for the Nan_natural catchment in 2011, which is part of the calibration period. The simulated streamflows obtained with different *KsatHorFrac* values from 100 to 800 for the PTF-B parameter set (panel (A)) and PTF-C parameter set (panel (B)) are presented as ranges in light colored bands. The simulated streamflows obtained with the optimized *KsatHorFrac* values are shown in solid colored lines, compared to the observations (obs) in dashed black lines.

5. Results

5.1. Parameter optimization and uncertainty

During the calibration of the *KsatHorFrac* parameter, we found that higher *KsatHorFrac* values generally attenuate the magnitude of streamflow, especially for peak flows, and flatten their recession limbs. With the same *KsatHorFrac* value, the PTF-B parameter set produces daily streamflow with steeper peaks and more rapid recessions than the PTF-C parameter set. This is because PTF-B presents more varying *KsatVer* values, with lower *M* values, over the study area (Fig. 3), resulting in less daily baseflow contribution. The optimized *KsatHorFrac* value for the upper GCPR basin is 550 for PTF-B and 120 for PTF-C. The range of the simulated daily streamflows with the *KsatHorFrac* values between 100 and 800 is more narrow for PTF-B than for PTF-C (light colored bands in Fig. 6), indicating that PTF-B introduces a smaller uncertainty in the streamflow results compared to PTF-C.

With their optimized *KsatHorFrac* values, PTF-B and PTF-C deliver similar estimates of daily streamflow for both natural and regulated catchments, as demonstrated by the colored lines in Fig. 6 and the goodness-of-fit indicators in Table 5. PTF-B outperforms PTF-C in the natural catchments, while PTF-C performs better in the regulated catchments. PTF-B tends to result in higher α, but smaller β compared to PTF-C, indicating a lower error in the variability (less overestimating or underestimating the variability in daily streamflow), but a larger bias (more overestimating or underestimating the mean streamflow). This is because PTF-B captures the daily streamflow fluctuation and magnitudes of daily peak flows more accurately whereas PTF-C is better at simulating daily baseflow, as also visible in Fig. 6.

5.2. Model performance in natural catchments

Overall, the wflow_sbm model with the global data and seamless distributed parameter maps can reconstruct the observed daily streamflow for the natural catchments. The daily hydrographs of the Nan_natural catchment (Fig. 7(A) and (B)) and Yom_natural catchment (Fig. 7(C) and (D)) show good fits in the peak timing and seasonal variability between the observed and simulated streamflows in both wet year (2006) and dry year (2013). Table 5 indicates satisfactory model performance, with the KGE value in the validation period ranging between 0.63 and 0.65 for the Nan_natural catchment and 0.78 for the Yom_natural catchment. Apart from the spatial uncertainty in model parameters, the varying model performances between the two catchments can be attributed to the difference in the catchment characteristics, particularly the elevation and land cover. A large part of the Nan_natural catchment is mountainous with forest areas, as shown in Figs. 1 and 4. Therefore, its hydrological processes are more difficult to simulate compared to the Yom_natural catchment that is less steep with more grasslands. The difficulty is caused by the higher amount and variability in precipitation, which result in the higher and more fluctuating streamflow, as also evident in Table 2. As a result, the peak flow magnitude in the Nan_natural catchment was five times higher than in the Yom_natural catchment in the wet year (Fig. 7(A) and (C)) and nine times higher in the dry year (Fig. 7(B) and (D)). For both catchments, the model tends to underestimate peak flows in the rainy season, especially at the beginning of the monsoon period, and miss peak flows generated by local storm events in the dry season.

5.3. Model performance in regulated catchments

The wflow_sbm model with the ROM shows varying performances when simulating the regulated streamflow for the Sirikit and Bhumibol catchments (Table 5). On the one hand, the daily streamflow estimate for the Sirikit catchment is passable, with the highest KGE of 0.43 (PTF-C) in the validation period. On the other hand, the model failed to estimate the daily streamflow for the Bhumibol catchment, resulting in negative KGE values in both calibration and validation periods. The major sources of error for both catchments are the inflexibility of the daily reservoir releases and the prompt releases of surcharge water by the ROM in the very wet periods, as evidenced in Fig. 7(E), (G) and (H). Therefore, the resulting accuracy for both reservoirs tends to be higher in the dry season than in the

Table 5
Wflow_sbm performance in simulating daily streamflow for the four study catchments and daily storage for the two reservoirs, with the PTF-B and PTF-C parameter sets. KGE and its components were obtained during the calibration (first row) and validation (second row) against observations. The model was calibrated for the years 2010–2011 and validated for the years 1989–2013, excluding 2010–2011.

		Period	PTF-B KGE	r	α	β	PTF-C KGE	r	α	β
Catchment (streamflow)	Nan_natural	Cal	**0.68**	0.89	0.85	0.73	**0.66**	0.89	0.80	0.74
		Val	**0.65**	0.85	0.88	0.70	**0.63**	0.83	0.83	0.71
	Yom_natural	Cal	**0.67**	0.80	0.78	0.86	**0.65**	0.79	0.75	0.87
		Val	**0.78**	0.79	1.07	0.97	**0.78**	0.78	0.96	0.97
	Sirikit	Cal	**0.24**	0.42	1.36	1.34	**0.25**	0.43	1.35	1.35
		Val	**0.41**	0.42	0.87	0.94	**0.43**	0.45	0.84	0.96
	Bhumibol	Cal	**-0.68**	0.04	2.06	1.88	**-0.63**	0.03	1.96	1.89
		Val	**-0.26**	0.04	1.73	1.37	**-0.21**	0.06	1.65	1.38
Reservoir (storage)	Sirikit	Cal	**0.45**	0.77	0.54	1.20	**0.41**	0.79	0.49	1.22
		Val	**0.80**	0.87	1.03	0.85	**0.81**	0.86	1.05	0.88
	Bhumibol	Cal	**0.13**	0.69	0.35	1.50	**0.12**	0.71	0.33	1.50
		Val	**0.59**	0.69	1.09	1.24	**0.59**	0.71	1.04	1.28

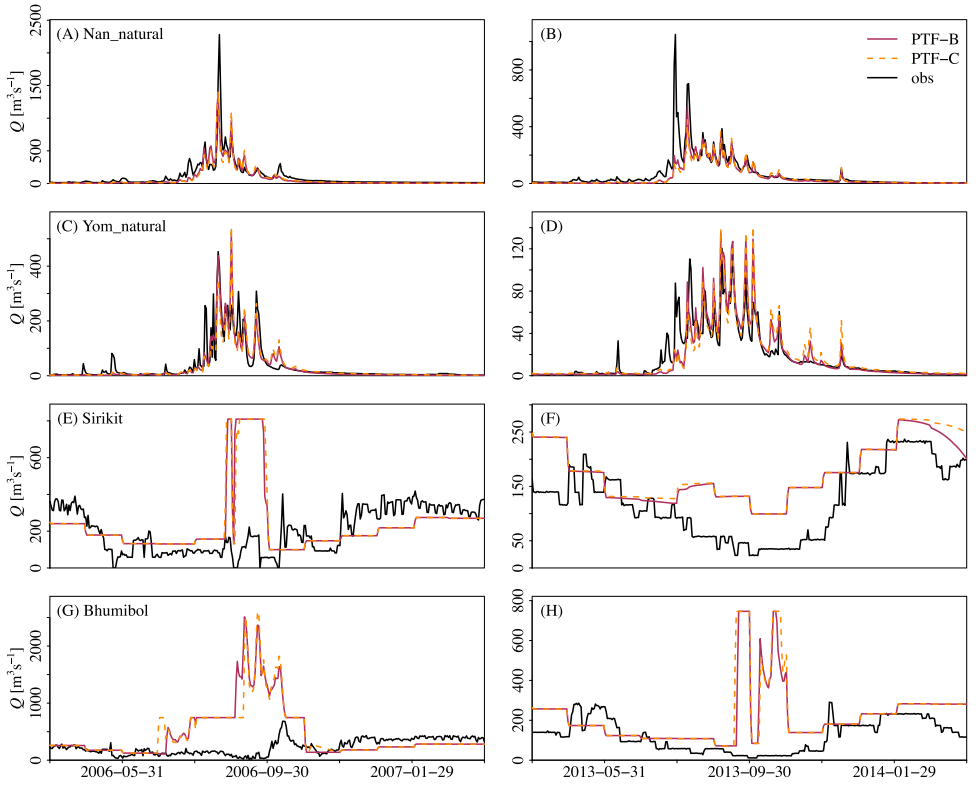

Fig. 7. Simulated and observed daily streamflows in the wet year (2006; left panels) and the dry year (2013; right panels) for the Nan_natural (first row), Yom_natural (second row), Sirikit (third row), and Bhumibol (bottom row) catchments. The simulated streamflow with the optimized PTF-B parameter set is shown in solid red lines, the simulated streamflow with the optimized PTF-C parameter set in dashed orange lines, and the observations (obs) in solid black lines.

rainy season, and higher in dry years than in wet years.

To elaborate the ROM performance, the daily water storage computed by the ROM for the Sirikit and Bhumibol reservoirs are compared to observations in Fig. 8. Overall, the simulated reservoir storage reasonably captures the inter- and intra-annual variability, although the magnitude is not accurate. The storage tends to be underestimated for the Sirikit reservoir and overestimated for the Bhumibol reservoir. In very wet periods, the storage is overestimated and exceeds the monthly target maximum (top of gray band in Fig. 8). This occurred more often for the Bhumibol reservoir than for the Sirikit reservoir, especially after the year 2003. As a result, the goodness-of-fit of the simulated storage (Table 5) is significantly better for the Sirikit reservoir (highest KGE = 0.81 with PTF-C) than

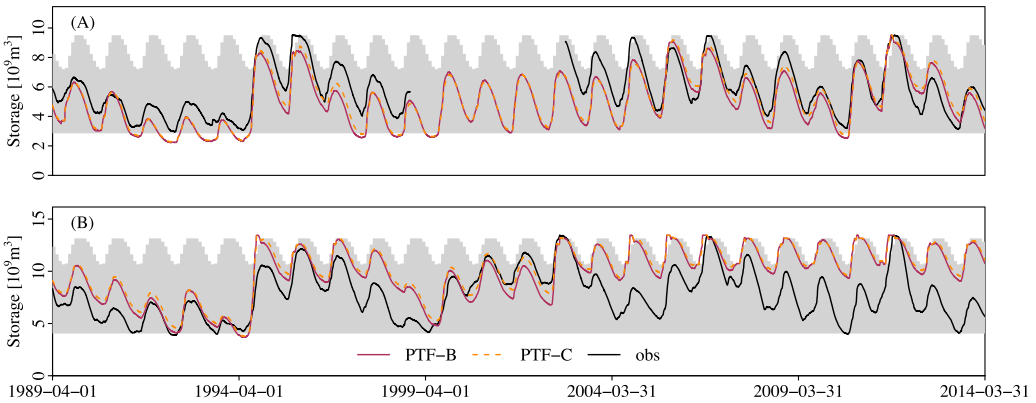

Fig. 8. Simulated and observed daily storages of the Sirikit reservoir (A) and the Bhumibol reservoir (B) during the years 1989–2013. The gray bands represent the ranges between the monthly target maximum storage and the target minimum storage, which was fixed as 30 percent of the reservoir capacity. The simulated storage with the optimized PTF-B parameter set is shown in solid red lines, the simulated storage with the optimized PTF-C parameter set in dashed orange lines, and the observations (obs) in solid black lines.

the Bhumibol reservoir (KGE = 0.59 for both PTF-B and for PTF-C). Due to the storage overestimation, the ROM released surcharge storage promptly (according to Eq. (7)), producing the unrealistic streamflow, as appeared in 2006 (Fig. 7(E) and (G)). Although the observed daily storage of both reservoirs also exceeded the monthly target maximum in some wet years, e.g., 1995, 2006 and 2011 (Fig. 8), most of observed surcharged water was allowed to stay in the reservoirs instead of being spilled at once. Therefore, the observed peak outflow due to surcharge storage was not as huge as the outflow simulated by the ROM (Fig. 7(E)–(H)). Due to the limited flexibility of the ROM, it cannot capture the dynamics of the observed reservoir releases at the daily timescale. However, it does show satisfactory performance at the monthly timescale (see the supplementary document).

6. Discussion

6.1. *wflow_sbm with global data and parameterization*

To our knowledge, this is the first study that applied the wflow_sbm model to simulate the daily streamflow in the upper GCPR basin. By setting up the model with global geospatial datasets (e.g., SRTM elevation), forcing the model with global meteorological datasets (MSWEP V2 *P* and eartH2Observe *PET*), and applying the seamless parameter maps based on SoilGrids, GLOBCOVER, and other global databases (e.g., MODIS LAI), we are able to circumvent the poor availability of in situ data often occurring in SEA. The seamless distributed parameter maps were applied to all but one sensitive soil-related parameter, *KsatHorFrac*, for which PTFs were unavailable (Imhoff et al., 2020). Although a full calibration procedure may improve the model performance, calibrating only one parameter prevented overparameterization and equifinality as well as reduced the computational time when simulating such a large basin at high spatial and temporal resolutions.

The model sensitivity to the soil-related parameter maps with different pedotransfer functions, PTF-B and PTF-C, became apparent due to the difference in the optimized *KsatHorFrac* values (550 for PTF-B and 120 for PTF-C). *KsatHorFrac* controls horizontal saturated conductivity, which influences the magnitude of the lateral subsurface flow and thus streamflow dynamics and recession after a peak (Fig. 6). The parameter is, therefore, sensitive to the other soil-related parameters, particularly *KsatVer* (vertical saturated conductivity) and *M* (decay rate of *KsatVer*) (see full description in Table 3). PTF-B and PTF-C produced very different spatial values of *KsatVer* and *M*, as visible in Fig. 3. Therefore, we suggest calibrating *KsatHorFrac* with respect to the selected PTF parameter set and study area. Furthermore, calibrating the *KsatHorFrac* based on soil types or elevation instead of calibrating it as a constant value may improve the model performance, which can benefit the model application for the real-time forecasting purpose, although more computational efforts are demanded. Nevertheless, the range of streamflows simulated with the *KsatHorFrac* values of 100–800 is not very large, especially for PTF-B (Fig. 6). Therefore, running the model without any calibration only introduces a little uncertainty, which makes it possible to apply it in ungauged basins.

Other sources of model uncertainty, such as the meteorological, geospatial, and hydrological input data, were not investigated in this study but could play a role in the model errors. Firstly, the synthetic meteorological data from global databases are subject to their own spatial (~10 km) and temporal (3 hourly–daily) resolutions, which were coarser than the target resolutions of the model (~1 km and 3 hourly). As a result, the *P* data failed to present local storm events, leading to the absence of local peak flows in dry seasons and in the beginning of rainy seasons for natural catchments (Fig. 7(A)–(D)). In a similar manner, the quality of the *PET* data directly affects the actual evapotranspiration (*AET*) estimates, but their accuracy was difficult to evaluate. Secondly, the seamless distributed maps for the land cover-related parameters were created based on the land cover database from the year 2009 (Fig. 4). In fact, the land cover in the upper GCPR basin has gradually changed over time, with decreasing forest areas and increasing agricultural areas (Jamrussri and Toda, 2017). Therefore, assigning the land cover-related parameters based on yearly land cover maps may improve the model results. Lastly, quality of the observed streamflow data was unverified and could also affect the model performance evaluation to some extent.

Considering the study purpose, we conclude that the wflow_sbm model with global data and parameterization is capable of simulating the daily streamflow for natural catchments (Fig. 7(A)–(D) and Table 5), but less effective for the regulated catchments due to limitations in the ROM (see Section 6.2 for more detail). In most study catchments, the goodness-of-fit results were higher during the validation than during the calibration potentially because the short calibration period (years 2010–2011) was both extremely wet and dry, while the validation period (years 1989–2013, excluding 2010–2011) also contained more regular hydrological conditions. Nonetheless, the wflow_sbm model outperforms the SWAT model that was run with observed daily meteorological data and fully calibrated for the same study area (Jamrussri and Toda, 2017). Therefore, it has potential to serve as a tool for the upper GCPR basin and other ungauged or data-scarce catchments in SEA.

6.2. *Reservoir operation module*

Reservoir operation modules with the target storage-and-release-based methods usually require a large amount of data for an individual reservoir that may be undocumented or difficult to obtain, particularly for data-scarce areas like SEA. Yassin et al. (2019) found that even when the required data are available, they usually contain considerable uncertainties so that optimizing operational parameters is still insufficient to represent the absolute storage-release relationship for many reservoirs, especially the multipurpose ones. Considering limited data available for the upper GCPR basin, the ROM was, therefore, designed to minimize the number of operational parameters and utilize accessible data without calibration (Fig. 5 and Table 4), which also allowed for investigating the data competence.

The main error in the ROM results was the daily storage that exceeded the monthly target maximum in the rainy seasons (Fig. 8). In response, the surcharge water was promptly released by the ROM, causing unrealistic flood peaks (Fig. 7(E), (G) and (H)), especially

for the Bhumibol reservoir. Meanwhile, the observations showed that the daily storage also exceeded the monthly target maximum in some wet years. However, the surcharge was not released at once, but was held and gradually released to prevent downstream floods. In some occasions, the daily releases were paused for a few days to control downstream floods. This indicates the high flexibility of the actual reservoir operations on a day-to-day basis, which could not be captured by the ROM that is based on the monthly operating rule curves and piece-wise linear regression algorithm. This flexibility reflects real-time decision making by dam operators to meet occasional targets, such as mitigating floods, satisfying downstream irrigation demands and increasing the hydropower generation (Yassin et al., 2019). Therefore, the ROM simulations in this study can be seen as the baseline operation scenario, which reflects the generalized operations without further impacts of human intervention. This baseline simulation is useful for analyzing effects of reservoir operations on downstream flows, which is presented in a companion paper (Wannasin et al., 2021). Although the real-time decision making is beyond the capability of the ROM and other mathematical operation modules, we suggest that the ROM performance can still be upgraded in the future with (i) a more accurate storage calculation and (ii) a more complex release algorithm.

The storage calculation may be improved with the higher accuracy of daily reservoir inflows and direct *AET* losses computed by the wflow_sbm model. In this study, the upstream inflows of the Sirikit and Bhumibol reservoirs were simulated as naturalized flows and indirectly validated with upstream flows since reliable reservoir inflow data are unavailable. However, there are four reservoirs located upstream of the Bhumibol reservoir, which have been operated since 2003. Therefore, the simulated inflows could be inaccurate, although this was impossible to evaluate without reliable observed data. This explains the storage overestimation for the Bhumibol reservoir after 2003 (Fig. 8(B)). Meanwhile, the inaccuracy of the daily *AET* could be partly due to simplification of the ROM itself. Since the water surface area of each reservoir was set as a fixed value (Table 1), despite the daily storage change, the amount of daily evaporating water could be under- or overestimated. Therefore, the reservoir area-elevation-storage relationship (e.g., Zhao et al., 2016b) may increase the accuracy of the daily *AET* losses and thus the daily storage estimated by the ROM.

The main factor determining the release algorithm in the ROM is the monthly target downstream water demand (*DD*). Without existing data, the *DD* of each reservoir was estimated as the long-term-monthly average of the reservoir outflow (Fig. 5), which could be a source of significant uncertainty for the daily outflow simulation. Another limitation of this algorithm is that it intends to meet the target *DD* without considering the daily inflows (e.g., thresholds for flooding, normal, and low inflows) or maximum acceptable streamflow at downstream control points (e.g., at Nakhon Sawan). Adding these factors into the outflow determination process (e.g., Zhao et al., 2016b; Yassin et al., 2019) may rectify the unrealistic surcharge releases. In addition, a release coefficient (e.g., annual coefficients as a function of mean total annual inflow) could introduce the inter-annual release variability into the module (Hanasaki et al., 2006). However, more parameters also mean more uncertainty sources and thus their competence should be carefully assessed.

6.3. Human impacts on hydrological modeling and streamflow

Our findings are in substantial agreement with previous studies, concluding that simulating the outflows of the Sirikit and Bhumibol reservoirs is challenging due to the complex patterns of real-time decision making by dam operators. Neither target storage-and-release-based methods nor inflow-and-demand-based methods applied in the past could satisfactorily reconstruct the actual operations of these two reservoirs at the daily timescale (e.g., Hanasaki et al., 2006; Mateo et al., 2014; Yassin et al., 2019). The recent study of Yassin et al. (2019) suggested that it was mainly due to the high ratio of the maximum reservoir storage and the mean total annual inflow of both reservoirs (>0.5), indicating more radical regulations compared to many other reservoirs worldwide. Moreover, since the outflows of the Sirikit and Bhimibol reservoirs conjugate at Nakhon Sawan, it is likely that both reservoirs are jointly operated in real time to manage floods and droughts in the downstream floodplain, as also reported during the 2011 GCPR flooding (Komori et al., 2012).

Recently, Yang et al. (2019) found that the data-driven method, artificial neural networks (ANNs), could learn the complex pattern of the observed reservoir outflow records and reproduce the daily outflow more accurately for both Sirikit (NSE = 0.93) and Bhumibol reservoirs (NSE = 0.86). Therefore, they can be useful tools for real-time reservoir outflow simulation and forecasting. However, since ANNs are black boxes, they cannot reveal the insights of real-time decision making in the actual operations of the reservoirs, which remain imperative for better and more sustainable reservoir water management in the future.

Above all, the unsatisfactory simulations of the reservoir outflows by the ROM reflect the strong and prompt human intervention on daily streamflow. In the areas that are at risks of floods and droughts like the upper GCPR basin and other basins in SEA, understanding of quantitative impacts of reservoir operations, especially with real-time decision making, on downstream flows is essential. Therefore, we further applied the developed model and results from this study to assess the effects of reservoir operations on the daily streamflow in the upper GCPR basin in a companion paper (Wannasin et al., 2021). With deeper knowledge on both reservoir system modeling and reservoir effects, we expect to be more capable of improving hydrological modeling and water resource management simultaneously.

7. Conclusion and outlook

This study concerned the development of a (~1 km resolution) distributed hydrological model, wflow_sbm, with global spatial data and parameterization and the exploration of its performance in estimating daily streamflow in the upper Greater Chao Phraya River basin. The main findings are as follows:

1. The global-data-driven wflow_sbm model can satisfactorily estimate daily streamflow in the natural catchments (highest KGE = 0.78 in the validation period).

2. The wflow_sbm model was not able to estimate daily streamflow in regulated catchments very well due to the simplified algorithm of the reservoir operation module (ROM) (highest KGE = 0.43 in the validation period).
3. The ROM with the (monthly) operation rules can capture the seasonal variability of the reservoir storage and releases, but cannot take into account real-time decision making by dam operators. The ROM results, therefore, reflect the baseline operations without further impacts of human intervention.
4. The difference between daily reservoir outflows from the baseline operation (simulations) and from the real-time operation (observations) highlights the strong effect and importance of real-time decision making to optimize the reservoir releases promptly, especially during extreme events. At the same time, it also addresses the source of difficulties in modeling large-scale multipurpose reservoirs. A more complex module with optimized parameters may improve the results, but uncertainties remain high.
5. With rooms for improvements, the proposed model can reasonably serve as a tool for analyzing catchment-scale hydrological variations in the GCPR basin and provide an opportunity for streamflow estimation in other ungauged or data-scarce basins in Southeast Asia.

Based on the findings, more studies on the use of seamless parameter maps based on global data for distributed hydrological modeling in other data-scarce basins are encouraged. Effects of using different global meteorological datasets on the model performance should also be explored. Future challenges in the reservoir system modeling include gaining a better understanding of the complexity of the real-time operations and improving the model performance for multipurpose reservoirs. A companion paper (Wannasin et al., 2021) describes the application of the global-data-driven wflow_sbm model with the ROM on investigating the reservoir operations and their effects on the daily flow regime in the same basin.

Declaration of competing interest

The authors declare that they have no known competing financial interests or personal relationships that could have appeared to influence the work reported in this paper.

Declaration of Competing Interest

The authors report no declarations of interest.

Acknowledgments

This research was supported by the Royal Thai Government Scholarship as part of the doctoral study of the first author. We would like to thank the Royal Irrigation Department of Thailand (RID) and the Electricity Generating Authority of Thailand (EGAT) for providing observational records. We received support from Kanjanawan Nilklud and Thattanaporn Khomsri in collecting the national and local reports used in this study. We benefited from the preliminary study of the reservoir operation module on the Sirikit reservoir conducted by Maarten Verbrugge. Our thanks also go to Ruben Imhoff and other experts at Deltares for their assistance with the wflow_sbm model and seamless distributed parameter maps.

Appendix A. Supplementary data

Supplementary data associated with this article can be found, in the online version, at https://doi.org/10.1016/j.ejrh.2021.100794.

References

Abbott, M.B., Bathurst, J.C., Cunge, J.A., O'Connell, P.E., Rasmussen, J., 1986. An introduction to the European Hydrological System – Systeme Hydrologique Europeen, "SHE", 1: History and philosophy of a physically-based, distributed modelling system. J. Hydrol. 87, 45–59. https://doi.org/10.1016/0022-1694(86)90114-9.

Ajami, N.K., Hornberger, G.M., Sunding, D.L., 2008. Sustainable water resource management under hydrological uncertainty. Water Resour. Res. 44 https://doi.org/10.1029/2007WR006736.

Allen, R.G., Pereira, L.S., Raes, D., Smith, M., et al., 1998. Crop Evapotranspiration-Guidelines for Computing Crop Water Requirements – FAO Irrigation and Drainage Paper 56. FAO, Rome 300, D05109.

Arnell, N.W., Gosling, S.N., 2016. The impacts of climate change on river flood risk at the global scale. Clim. Change 134, 387–401. https://doi.org/10.1007/s10584-014-1084-5.

Bachelet, D., Brown, D., Böhm, M., Russell, P., 1992. Climate change in Thailand and its potential impact on rice yield. Clim. Change 21, 347–366. https://doi.org/10.1007/BF00141376.

Bagley, J.E., Desai, A.R., Harding, K.J., Snyder, P.K., Foley, J.A., 2014. Drought and deforestation: has land cover change influenced recent precipitation extremes in the Amazon? J. Clim. 27, 345–361. https://doi.org/10.1175/JCLI-D-12-00369.1.

Beck, H.E., Vergopolan, N., Pan, M., Levizzani, V., Van Dijk, A.I., Weedon, G.P., Brocca, L., Pappenberger, F., Huffman, G.J., Wood, E.F., 2017. Global-scale evaluation of 22 precipitation datasets using gauge observations and hydrological modeling. Hydrol. Earth Syst. Sci. 21 (12), 6201–6217. https://doi.org/10.5194/hess-21-6201-2017.

Beck, H.E., Wood, E.F., McVicar, T.R., Zambrano-Bigiarini, M., Alvarez-Garreton, C., Baez-Villanueva, O.M., Sheffield, J., Karger, D.N., 2020. Bias correction of global high-resolution precipitation climatologies using streamflow observations from 9372 catchments. J. Clim. 33, 1299–1315. https://doi.org/10.1175/JCLI-D-19-0332.1.

Beck, H.E., Wood, E.F., Pan, M., Fisher, C.K., Miralles, D.G., Van Dijk, A.I., McVicar, T.R., Adler, R.F., 2019. MSWEP V2 global 3-hourly 0.1° precipitation: methodology and quantitative assessment. Bull. Am. Meteorol. Soc. 100, 473–500. https://doi.org/10.1175/BAMS-D-17-0138.1.

Bell, V.A., Kay, A.L., Jones, R.G., Moore, R.J., 2007. Development of a high resolution grid-based river flow model for use with regional climate model output. Hydrol. Earth Syst. Sci. 11 (1), 532–549. https://doi.org/10.5194/hess-11-532-2007.

Beven, K., 2006. A manifesto for the equifinality thesis. J. Hydrol. 320, 18–36. https://doi.org/10.1016/j.jhydrol.2005.07.007.

Beven, K.J., Kirkby, M.J., 1979. A physically based, variable contributing area model of basin hydrology/un modèle à base physique de zone d'appel variable de l'hydrologie du bassin versant. Hydrol. Sci. J. 24, 43–69. https://doi.org/10.1080/02626667909491834.

Bhagabati, S.S., Kawasaki, A., 2017. Consideration of the rainfall-runoff-inundation (RRI) model for flood mapping in a deltaic area of Myanmar. Hydrol. Res. Lett. 11, 155–160. https://doi.org/10.3178/hrl.11.155.

Bontemps, S., Defourny, P., Van Bogaert, E., Arino, O., Kalogirou, V., Perez, J.R., 2011. GLOBCOVER 2009-Products Description and Validation Report. The European Space Agency GlobCover Portal (last accessed on 15/07/2020). http://due.esrin.esa.int/page_globcover.php.

Brakensiek, D., Rawls, W., Stephenson, G., 1984. Modifying SCS Hydrologic Soil Groups and Curve Numbers for Rangeland Soils. American Society of Agricultural Engineers.

Brooks, E.S., Boll, J., McDaniel, P.A., 2004. A hillslope-scale experiment to measure lateral saturated hydraulic conductivity. Water Resour. Res. 40 https://doi.org/10.1029/2003WR002858.

Brooks, R.H., Corey, A.T., 1964. Hydraulic Properties of Porous Media. Colorado State University, pp. 1–27, 3, Hydrol, Paper.

Calver, A., Cammeraat, L., 1993. Testing a physically-based runoff model against field observations on a Luxembourg hillslope. Catena 20, 273–288. https://doi.org/10.1016/0341-8162(93)90005-A.

Ceola, S., Laio, F., Montanari, A., 2014. Satellite nighttime lights reveal increasing human exposure to floods worldwide. Geophys. Res. Lett. 41, 7184–7190. https://doi.org/10.1002/2014GL061859.

Chang, H., Franczyk, J., 2008. Climate change, land-use change, and floods: toward an integrated assessment. Geogr. Compass 2, 1549–1579. https://doi.org/10.1111/j.1749-8198.2008.00136.x.

Cloke, H., Pappenberger, F., 2009. Ensemble flood forecasting: a review. J. Hydrol. 375, 613–626. https://doi.org/10.1016/j.jhydrol.2009.06.005.

Cook, E.R., Anchukaitis, K.J., Buckley, B.M., D'Arrigo, R.D., Jacoby, G.C., Wright, W.E., 2010. Asian monsoon failure and megadrought during the last millennium. Science 328, 486–489. https://doi.org/10.1126/science.1185188.

Cosby, B., Hornberger, G., Clapp, R., Ginn, T., 1984. A statistical exploration of the relationships of soil moisture characteristics to the physical properties of soils. Water Resour. Res. 20, 682–690. https://doi.org/10.1029/WR020i006p00682.

Crawford, N.H., 1966. Digital Simulation in Hydrology: Stanford Watershed Model IV. Stanford Univ. Tech. Report. 39, Stanford, US.

Dai, A., 2011. Drought under global warming: a review. Wiley Interdiscip. Rev.: Clim. Change 2, 45–65. https://doi.org/10.1002/wcc.81.

Dai, A., 2013. Increasing drought under global warming in observations and models. Nat. Clim. Change 3, 52. https://doi.org/10.1038/nclimate1633.

Engman, E.T., 1986. Roughness coefficients for routing surface runoff. J. Irrig. Drain. Eng. 112, 39–53. https://doi.org/10.1061/(ASCE)0733-9437(1986)112:1(39).

Fortin, J.P., Turcotte, R., Massicotte, S., Moussa, R., Fitzback, J., Villeneuve, J.P., 2001. Distributed watershed model compatible with remote sensing and GIS data. I: Description of model. J. Hydrol. Eng. 6, 91–99. https://doi.org/10.1061/(ASCE)1084-0699(2001)6:2(91).

Gash, J., 1979. An analytical model of rainfall interception by forests. Q. J. R. Meteorol. Soc. 105, 43–55. https://doi.org/10.1002/qj.49710544304.

Gauthier, M.J., Camporese, M., Rivard, C., Paniconi, C., Larocque, M., 2009. A modeling study of heterogeneity and surface water-groundwater interactions in the Thomas Brook catchment, Annapolis Valley (Nova Scotia, Canada). Hydrol. Earth Syst. Sci. 13, 1583–1596. https://doi.org/10.5194/hess-13-1583-2009.

Gebremicael, T., Mohamed, Y., Van der Zaag, P., 2019. Attributing the hydrological impact of different land use types and their long-term dynamics through combining parsimonious hydrological modelling, alteration analysis and PLSR analysis. Sci. Total Environ. 660, 1155–1167. https://doi.org/10.1016/j.scitotenv.2019.01.085.

Giardino, A., Schrijvershof, R., Nederhoff, C., De Vroeg, H., Brière, C., Tonnon, P.K., Caires, S., Walstra, D., Sosa, J., Van Verseveld, W., et al., 2018. A quantitative assessment of human interventions and climate change on the West African sediment budget. Ocean Coast. Manag. 156, 249–265. https://doi.org/10.1016/j.ocecoaman.2017.11.008.

Gourley, J.J., Vieux, B.E., 2006. A method for identifying sources of model uncertainty in rainfall-runoff simulations. J. Hydrol. 327, 68–80. https://doi.org/10.1016/j.jhydrol.2005.11.036.

Grayson, R., Blöschl, G., 2001. Spatial Modelling of Catchment Dynamics. Cambridge University Press, Cambridge, UK.

Gupta, H.V., Kling, H., Yilmaz, K.K., Martinez, G.F., 2009. Decomposition of the mean squared error and NSE performance criteria: implications for improving hydrological modelling. J. Hydrol. 377, 80–91. https://doi.org/10.1016/j.jhydrol.2009.08.003.

Hanasaki, N., Kanae, S., Oki, T., 2006. A reservoir operation scheme for global river routing models. J. Hydrol. 327, 22–41. https://doi.org/10.1016/j.jhydrol.2005.11.011.

Hassaballah, K., Mohamed, Y., Uhlenbrook, S., Biro, K., 2017. Analysis of streamflow response to land use and land cover changes using satellite data and hydrological modelling: case study of Dinder and Rahad tributaries of the Blue Nile (Ethiopia-Sudan). Hydrol. Earth Syst. Sci. 21, 5217. https://doi.org/10.5194/hess-21-5217-2017.

Hengl, T., de Jesus, J.M., Heuvelink, G.B., Gonzalez, M.R., Kilibarda, M., Blagotić, A., Shangguan, W., Wright, M.N., Geng, X., Bauer-Marschallinger, B., et al., 2017. SoilGrids250m: global gridded soil information based on machine learning. PLoS One 12. https://doi.org/10.1371/journal.pone.0169748.

Hirabayashi, Y., Mahendran, R., Koirala, S., Konoshima, L., Yamazaki, D., Watanabe, S., Kim, H., Kanae, S., 2013. Global flood risk under climate change. Nat. Clim. Change 3, 816. https://doi.org/10.1038/nclimate1911.

Imhoff, R., van Verseveld, W., van Osnabrugge, B., Weerts, A., 2020. Scaling point-scale (pedo) transfer functions to seamless large-domain parameter estimates for high-resolution distributed hydrologic modeling: an example for the Rhine river. Water Resour. Res. 56 https://doi.org/10.1029/2019WR026807.

Jamrussri, S., Toda, Y., 2017. Simulating past severe flood events to evaluate the effectiveness of nonstructural flood countermeasures in the upper Chao Phraya River Basin, Thailand. J. Hydrol.: Reg. Stud. 10, 82–94. https://doi.org/10.1016/j.ejrh.2017.02.001.

Jarvis, A., Reuter, H.I., Nelson, A., Guevara, E., 2008. Hole-Filled Seamless SRTM Data V4. International Centre for Tropical Agriculture (CIAT) (last accessed on 15/07/2020). http://srtm.csi.cgiar.org.

Kilgore, J.L., 1997. Development and Evaluation of a GIS-Based Spatially Distributed Unit Hydrograph Model. Virginia Tech. Master thesis.

Kinouchi, T., Yamamoto, G., Komsai, A., Liengcharernsit, W., 2018. Quantification of seasonal precipitation over the upper Chao Phraya River Basin in the past fifty years based on monsoon and El Niño/Southern Oscillation Related Climate Indices. Water 10, 800. https://doi.org/10.3390/w10060800.

Kite, G., 2000. Developing a Hydrological Model for the Mekong Basin: Impacts of Basin Development on Fisheries Productivity. International Water Management Institute, Colombo, Sri Lanka. IWMI Working Paper 2.

Kite, G., 2001. Modelling the Mekong: hydrological simulation for environmental impact studies. J. Hydrol. 253, 1–13. https://doi.org/10.1016/S0022-1694(01)00396-1.

Komori, D., Nakamura, S., Kiguchi, M., Nishijima, A., Yamazaki, D., Suzuki, S., Kawasaki, A., Oki, K., Oki, T., 2012. Characteristics of the 2011 Chao Phraya River flood in central Thailand. Hydrol. Res. Lett. 6, 41–46. https://doi.org/10.3178/hrl.6.41.

Kripalani, R., Singh, S., Panchawagh, N., Brikshavana, M., 1995. Variability of the summer monsoon rainfall over Thailand—comparison with features over India. Int. J. Climatol. 15, 657–672. https://doi.org/10.1002/joc.3370150606.

Kure, S., Tebakari, T., 2012. Hydrological impact of regional climate change in the Chao Phraya River Basin, Thailand. Hydrol. Res. Lett. 6, 53–58. https://doi.org/10.3178/hrl.6.53.

Li, R., Shi, J., Ji, D., Zhao, T., Plermkamon, V., Moukomla, S., Kuntiyawichai, K., Kruasilp, J., 2019. Evaluation and hydrological application of TRMM and GPM precipitation products in a tropical monsoon basin of Thailand. Water 11, 818. https://doi.org/10.3390/w11040818.
Lindström, G., Johansson, B., Persson, M., Gardelin, M., Bergström, S., 1997. Development and test of the distributed HBV-96 hydrological model. J. Hydrol. 201, 272–288.
Liu, S., 1998. Estimation of rainfall storage capacity in the canopies of cypress wetlands and slash pine uplands in North-Central Florida. J. Hydrol. 207, 32–41. https://doi.org/10.1016/S0022-1694(98)00115-2.
Liu, Z., Martina, M.L., Todini, E., 2005. Flood forecasting using a fully distributed model: application of the TOPKAPI model to the upper Xixian Catchment. Hydrol. Earth Syst. Sci. 9, 347–364. https://doi.org/10.5194/hess-9-347-2005.
Liu, X., Liu, F.M., Wang, X.X., Li, X.D., Fan, Y.Y., Cai, S.X., Ao, T.Q., 2017. Combining rainfall data from rain gauges and TRMM in hydrological modelling of Laotian data-sparse basins. Appl. Water Sci. 7, 1487–1496. https://doi.org/10.1007/s13201-015-0330-y.
Liu, J., Shangguan, D., Liu, S., Ding, Y., Wang, S., Wang, X., 2019. Evaluation and comparison of CHIRPS and MSWEP daily-precipitation products in the Qinghai-Tibet Plateau during the period of 1981–2015. Atmos. Res. 230, 104634. https://doi.org/10.1016/j.atmosres.2019.104634.
Livneh, B., Rajagopalan, B., Kasprzyk, J., et al., 2017. Hydrological model application under data scarcity for multiple watersheds, Java Island, Indonesia. J. Hydrol.: Reg. Stud. 9, 127–139. https://doi.org/10.1016/j.ejrh.2016.09.007.
López López, P., 2018. Application of Global Hydrological Datasets for River Basin Modelling. Utrecht University, Utrecht, the Netherlands, pp. 1–214. Doctoral dissertation.
López López, P., Wanders, N., Schellekens, J., Renzullo, L.J., Sutanudjaja, E., Bierkens, M.F., 2016. Improved large-scale hydrological modelling through the assimilation of streamflow and downscaled satellite soil moisture observations. Hydrol. Earth Syst. Sci. 20, 3059–3076. https://doi.org/10.5194/hess-20-3059-2016.
Luu, C., Von Meding, J., Kanjanabootra, S., 2018. Assessing flood hazard using flood marks and analytic hierarchy process approach: a case study for the 2013 flood event in Quang Nam, Vietnam. Nat. Hazards 90, 1031–1050. https://doi.org/10.1007/s11069-017-3083-0.
Mateo, C.M., Hanasaki, N., Komori, D., Tanaka, K., Kiguchi, M., Champathong, A., Sukhapunnaphan, T., Yamazaki, D., Oki, T., 2014. Assessing the impacts of reservoir operation to floodplain inundation by combining hydrological, reservoir management, and hydrodynamic models. Water Resour. Res. 50, 7245–7266. https://doi.org/10.1002/2013WR014845.
Myneni, R., Knyazikhin, Y., Park, T., 2015. MOD15A2H MODIS/terra Leaf Area Index/FPAR 8-day L4 global 500 m SIN grid V006 [Data set]. NASA EOSDIS Land Processes DAAC. https://doi.org/10.5067/MODIS/MOD15A2H.006.
Myo Lin, N., Rutten, M., Tian, X., 2018. Flood mitigation through optimal operation of a multi-reservoir system by using model predictive control: a case study in Myanmar. Water 10, 1371. https://doi.org/10.3390/w10101371.
Mysiak, J., Giupponi, C., Rosato, P., 2005. Towards the development of a decision support system for water resource management. Environ. Model. Softw. 20, 203–214. https://doi.org/10.1016/j.envsoft.2003.12.019.
Pitman, J.I., 1989. Rainfall interception by bracken in open habitats – relations between leaf area, canopy storage and drainage rate. J. Hydrol. 105, 317–334. https://doi.org/10.1016/0022-1694(89)90111-X.
Rawls, W., Brakensiek, D., 1989. Estimation of soil water retention and hydraulic properties. Unsaturated Flow in Hydrologic Modeling. Springer, pp. 275–300. https://doi.org/10.1007/978-94-009-2352-2_10.
Refsgaard, J.C., 1997. Parameterisation, calibration and validation of distributed hydrological models. J. Hydrol. 198, 69–97. https://doi.org/10.1016/S0022-1694(96)03329-X.
Refsgaard, J.C., Knudsen, J., 1996. Operational validation and intercomparison of different types of hydrological models. Water Resour. Res. 32, 2189–2202. https://doi.org/10.1029/96WR00896.
Rutter, A., Kershaw, K., Robins, P., Morton, A., 1971. A predictive model of rainfall interception in forests, 1. Derivation of the model from observations in a plantation of Corsican pine. Agric. Meteorol. 9, 367–384. https://doi.org/10.1016/0002-1571(71)90034-3.
Rutter, A., Morton, A., Robins, P., 1975. A predictive model of rainfall interception in forests. II. Generalization of the model and comparison with observations in some coniferous and hardwood stands. J. Appl. Ecol. 367–380. https://doi.org/10.2307/2401739.
Samaniego, L., Kumar, R., Attinger, S., 2010. Multiscale parameter regionalization of a grid-based hydrologic model at the mesoscale. Water Resour. Res. 46 https://doi.org/10.1029/2008WR007327.
Sayama, T., Tatebe, Y., Iwami, Y., Tanaka, S., 2015. Hydrologic sensitivity of flood runoff and inundation: 2011 Thailand floods in the Chao Phraya River basin. Nat. Hazards Earth Syst. Sci. 15, 1617–1630. https://doi.org/10.5194/nhess-15-1617-2015.
Schellekens, J., Dutra, E., la Torre, A.M.d., Balsamo, G., van Dijk, A., Weiland, F.S., Minvielle, M., Calvet, J.C., Decharme, B., Eisner, S., et al., 2017. A global water resources ensemble of hydrological models: the eartH2Observe Tier-1 dataset. Earth Syst. Sci. Data 9, 389–413. https://doi.org/10.5194/essd-2016-55.
Schellekens, J., Verseveld van, W., Euser, T., Winsemius, H., Thiange, C., Bouaziz, L., et al., 2019. Openstreams/wflow: Unstable-Master (last accessed on 15/07/2020). https://github.com/openstreams/wflow.
Singh, V.P., Woolhiser, D.A., 2002. Mathematical modeling of watershed hydrology. J. Hydrol. Eng. 7, 270–292. https://doi.org/10.1061/(ASCE)1084-0699(2002)7:4(270.
Skidmore, A., 2017. Environmental Modelling with GIS and Remote Sensing. CRC Press, pp. 1–259.
Sperna Weiland, F., Lopez Lopez, P., Van Dijk, A., Schellekens, J., et al., 2015. Global High-Resolution Reference Potential Evaporation. 21st Int. Congr. Model. Simul., pp. 2548–2554
Takeda, M., Laphimsing, A., Putthividhya, A., 2016. Dry season water allocation in the Chao Phraya River basin, Thailand. Int. J. Water Resour. Dev. 32, 321–338. https://doi.org/10.1080/07900627.2015.1055856.
Tarnavsky, E., Chavez, E., Boogaard, H., 2018. Agro-meteorological risks to maize production in Tanzania: sensitivity of an adapted Water Requirements Satisfaction Index (WRSI) model to rainfall. Int. J. Appl. Earth Observ. Geoinf. 73, 77–87. https://doi.org/10.1016/j.jag.2018.04.008.
Thanapakpawin, P., Richey, J., Thomas, D., Rodda, S., Campbell, B., Logsdon, M., 2007. Effects of landuse change on the hydrologic regime of the Mae Chaem river basin, NW Thailand. J. Hydrol. 334, 215–230. https://doi.org/10.1016/j.jhydrol.2006.10.012.
Todini, E., Ciarapica, L., 2002. The TOPKAPI Model. Mathematical Models of Large Watershed Hydrology. Water Resources Publications Edition.
Tóth, B., Weynants, M., Nemes, A., Makó, A., Bilas, G., Tóth, G., 2015. New generation of hydraulic pedotransfer functions for Europe. Eur. J. Soil Sci. 66, 226–238. https://doi.org/10.1111/ejss.12192.
Trenberth, K.E., Dai, A., Van Der Schrier, G., Jones, P.D., Barichivich, J., Briffa, K.R., Sheffield, J., 2014. Global warming and changes in drought. Nat. Clim. Change 4, 17–22. https://doi.org/10.1038/nclimate2067.
Van Dijk, A., Bruijnzeel, L., 2001. Modelling rainfall interception by vegetation of variable density using an adapted analytical model. Part 2. Model validation for a tropical upland mixed cropping system. J. Hydrol. 247, 239–262. https://doi.org/10.1016/S0022-1694(01)00393-6.
Van Looy, K., Bouma, J., Herbst, M., Koestel, J., Minasny, B., Mishra, U., Montzka, C., Nemes, A., Pachepsky, Y.A., Padarian, J., et al., 2017. Pedotransfer functions in Earth system science: challenges and perspectives. Rev. Geophys. 55, 1199–1256. https://doi.org/10.1002/2017RG000581.
Vertessy, R.A., Elsenbeer, H., 1999. Distributed modeling of storm flow generation in an Amazonian rain forest catchment: effects of model parameterization. Water Resour. Res. 35, 2173–2187. https://doi.org/10.1029/1999WR900051.
Vo, N.D., Gourbesville, P., 2016. Application of deterministic distributed hydrological model for large catchment: a case study at Vu Gia Thu Bon catchment, Vietnam. J. Hydroinf. 18, 885–904. https://doi.org/10.2166/hydro.2016.138.
Wang, W., Lu, H., Yang, D., Sothea, K., Jiao, Y., Gao, B., Peng, X., Pang, Z., 2016. Modelling hydrologic processes in the Mekong River Basin using a distributed model driven by satellite precipitation and rain gauge observations. PloS One 11. https://doi.org/10.1371/journal.pone.0152229.
Wannasin, C., Brauer, C., Uijlenhoet, R., van Verseveld, W., Weerts, A., 2021. Daily flow simulation in Thailand Part II: unraveling effects of reservoir operation. Hydrol.: Reg. Stud. https://doi.org/10.1016/j.ejrh.2021.100792.

Ward, P.J., Jongman, B., Weiland, F.S., Bouwman, A., van Beek, R., Bierkens, M.F., Ligtvoet, W., Winsemius, H.C., 2013. Assessing flood risk at the global scale: model setup, results, and sensitivity. Environ. Res. Lett. 8, 044019. https://doi.org/10.1088/1748-9326/8/4/044019.

Weedon, G.P., Balsamo, G., Bellouin, N., Gomes, S., Best, M.J., Viterbo, P., 2014. The WFDEI meteorological forcing data set: WATCH Forcing Data methodology applied to ERA-Interim reanalysis data. Water Resour. Res. 50, 7505–7514. https://doi.org/10.1002/2014WR015638.

Weiler, M., McDonnell, J., 2007. Conceptualizing lateral preferential flow and flow networks and simulating the effects on gauged and ungauged hillslopes. Water Resour. Res. 43 https://doi.org/10.1029/2006WR004867.

Wicks, J., Bathurst, J., 1996. SHESED: a physically based, distributed erosion and sediment yield component for the SHE hydrological modelling system. J. Hydrol. 175, 213–238. https://doi.org/10.1016/S0022-1694(96)80012-6.

Winsemius, H.C., Aerts, J.C., van Beek, L.P., Bierkens, M.F., Bouwman, A., Jongman, B., Kwadijk, J.C., Ligtvoet, W., Lucas, P.L., Van Vuuren, D.P., et al., 2016. Global drivers of future river flood risk. Nat. Clim. Change 6, 381. https://doi.org/10.1038/nclimate2893.

Xu, Z., Wu, Z., He, H., Wu, X., Zhou, J., Zhang, Y., Guo, X., 2019. Evaluating the accuracy of MSWEP V2.1 and its performance for drought monitoring over mainland China. Atmos. Res. 226, 17–31. https://doi.org/10.1016/j.atmosres.2019.04.008.

Yang, S., Yang, D., Chen, J., Zhao, B., 2019. Real-time reservoir operation using recurrent neural networks and inflow forecast from a distributed hydrological model. J. Hydrol. 579, 124229. https://doi.org/10.1016/j.jhydrol.2019.124229.

Yassin, F., Razavi, S., Elshamy, M., Davison, B., Sapriza-Azuri, G., Wheater, H., 2019. Representation and improved parameterization of reservoir operation in hydrological and land-surface models. Hydrol. Earth Syst. Sci. 23, 3735–3764. https://doi.org/10.5194/hess-23-3735-2019.

Yuan, F., Zhang, L., Soe, K.M.W., Ren, L., Zhao, C., Zhu, Y., Jiang, S., Liu, Y., 2019. Applications of TRMM-and GPM-era multiple-satellite precipitation products for flood simulations at sub-daily scales in a sparsely gauged watershed in Myanmar. Remote Sens. 11, 140. https://doi.org/10.3390/rs11020140.

Zajac, Z., Revilla-Romero, B., Salamon, P., Burek, P., Hirpa, F.A., Beck, H., 2017. The impact of lake and reservoir parameterization on global streamflow simulation. J. Hydrol. 548, 552–568. https://doi.org/10.1016/j.jhydrol.2017.03.022.

Zeng, X., 2001. Global vegetation root distribution for land modeling. J. Hydrometeorol. 2, 525–530. https://doi.org/10.1175/1525-7541(2001)002<0525:GVRDFL>2.0.CO;2.

Zhao, C., Shao, M., Jia, X., Nasir, M., Zhang, C., 2016a. Using pedotransfer functions to estimate soil hydraulic conductivity in the Loess Plateau of China. Catena 143, 1–6. https://doi.org/10.1016/j.catena.2016.03.037.

Zhao, G., Gao, H., Naz, B.S., Kao, S.C., Voisin, N., 2016b. Integrating a reservoir regulation scheme into a spatially distributed hydrological model. Adv. Water Resour. 98, 16–31. https://doi.org/10.1016/j.advwatres.2016.10.014.